2008:40

LICENTIATE THESIS

Physically Based Model for Plasticity and Creep of Ti-6Al-4V

Bijish Babu

Luleå University of Technology
Department of Applied Physics and Mechanical Engineering
Division of Material Mechanics

2008:40 | ISSN: 1402-1757 | ISRN: LTU-LIC -- 08/40 -- SE

LICENTIATE THESIS

Physically Based Model for Plasticity and Creep of Ti-6Al-4V

Bijish Babu

Division of Material Mechanics
Department of Applied Physics and Mechanical Engineering
Luleå University of Technology
SE-971 87 Luleå Sweden

Physically Based Model for Plasticity and Creep of Ti-6Al-4V
Bijish Babu

Licentiate Thesis 2008:40
ISSN:402-1757
ISRN:LTU-LIC – 08/40 – SE

Division of Material Mechanics
Department of Applied Physics and Mechanical Engineering
Luleå University of Technology
SE-971 87 Luleå Sweden
Phone: +46 (0)920 491824
11th December 2008

Abstract

Albeit Ti-6Al-4V has numerous salient properties, its usage for certain applications is limited due to the challenges faced during manufacturing. Understanding the dominant deformation mechanisms and numerically modelling the process is the key to overcome this hurdle. This work investigates plastic deformation of the alloy at strain rates from $0.001s^{-1}$ to $1s^{-1}$ and temperatures between 20 °C and 1100 °C. Pertinent deformation mechanisms of the material when subjected to thermo-mechanical processing is discussed. A physically based constitutive model based on the evolution of immobile dislocation density and excess vacancy concentration is developed. Parameters of the model are obtained by calibration using isothermal compression tests. Model is compared with relaxation test data to demonstrate its validity.

Acknowledgment

This work has been carried out at the division of Material Mechanics at Luleå University of Technology. Financial support was provided by the VERDI[†] project within the 6^{th} framework programme of the EU. I would like to express my sincere gratitude to my supervisor, Prof. Lars-Erik Lindgren for his enthusiasm and support during the course of this work. Many thanks to all my colleagues at the University for making the work inspiring.

[†]Virtual Engineering for Robust-manufacturing with Design Integration (http://verdi-fp6.org)

Publications

The work done in this thesis has been published in three scientific articles which are appended at the end.

Paper I
Dislocation density based constitutive model for Ti-6Al-4V at low strain rates. Bijish Babu, *Proceedings of the 11th World Conference on Titanium (Ti-2007).* Kyoto. December-2007. p311-314. ISBN:978-4-88903-406-6

This paper summarises the initial attempt to model the plastic flow of Ti-6Al-4V at low strain rates using a physically based model. This simple model could produce good fit to the test data.

Paper II
Dislocation density based constitutive model for Ti-6Al-4V: including recovery and recrystallisation. Bijish Babu, *Computational plasticity: Fundamentals and Applications (COMPLAS IX).* Barcelona. September-2007. p631-634. ISBN:978-84-96736-29-0

In this work, the model in Paper I is extended with a model for Dynamic Recrystallisation. Though this approach gave satisfactory predictions at different temperatures, the lack of quantitative data regarding the rate of recrystallisation proved to be a hindrance.

Paper III
Physically based model for plasticity and creep of Ti-6Al-4V. Bijish Babu. *Submitted to the Journal; Mechanics of Materials.* October-2008

This work extends the simple model in Paper I with a more advanced model. The enhanced diffusivity of the material driven by the short circut pipe diffusion is included. This model can predict the flow stress for a broad range of temperatures and strain rates. Additionally, the capacity of the model to compute stress relaxation is demonstrated, thereby unifying plasticity and creep in a single model.

Definitions

Some of the terms used in this thesis can have very vague and distinct definitions in the dictionary and reference books. Therefore in order to remove the ambiguity, a contextual definition is provided here.

Model: A simplified numerical abstraction of a physical process or phenomena used for predictions which can be collection of various sub-models.
In this work, the flow stress model is a combination of various sub-models, viz; diffusion, dislocation glide, dislocation climb, etc.

Simulation: Simulation is the imitation of a phenomena, process or activity which involves representing certain key characteristics or behaviors of a selected physical or abstract system.
In this work, simulation is defined as, a model put to useful work.

Microstructure: The microstructure of a material is the description of the crystal structure, chemical composition, orientation, distribution of defects, formation and arrangement of the lattice (morphology) etc.
In this work, this term has been used loosely to describe one or more of the above.

Adequate Accuracy: Simulations involve the usage of many simplifying assumptions and approximations which might deteriorate the accuracy of the prediction. When performing complex multiphysics simulations, it is required to arrive at a compromise between the quality of the prediction and complexity of the model. Therefore, the accuracy requirement on the model depends on its intented use.
In this work, since the quantitative estimation of the simulation error is not performed, adequate accuracy is used qualitatively to describe the capacity of the model to be used in simulations of forming, welding and heat treatment.

Contents

1 Introduction **1**
- 1.1 Background . . . 1
- 1.2 Scope of this work . . . 2

2 Deformation Mechanisms of Polycrystals **3**
- 2.1 Point Defects . . . 4
- 2.2 Line defects . . . 4
  - 2.2.1 Jogs and Kinks . . . 5
- 2.3 Planar defects . . . 5
- 2.4 Plasticity . . . 6
  - 2.4.1 Hardening Process . . . 6
  - 2.4.2 Restoration Processes . . . 7
- 2.5 Creep . . . 10
  - 2.5.1 Dislocation Creep . . . 10
  - 2.5.2 Nabarro-Herring Creep . . . 11
  - 2.5.3 Coble Creep . . . 11
  - 2.5.4 Granular Shear . . . 12
  - 2.5.5 Granular Fracture . . . 12

3 Ti-6Al-4V Microstructure and Properties **13**
- 3.1 Phase Evolution . . . 14
  - 3.1.1 The Primary phases (α, β) . . . 14
  - 3.1.2 The metastable phases ($\alpha\prime$, $\alpha\prime\prime$) . . . 15
  - 3.1.3 The Intermetalic phase (α_2) . . . 16
- 3.2 Plastic flow . . . 16
  - 3.2.1 Strain rate sensitivity . . . 16
  - 3.2.2 Hall-Petch Relation . . . 17
  - 3.2.3 Twinning . . . 18
  - 3.2.4 Flow Softening . . . 18
  - 3.2.5 Localisation . . . 20
- 3.3 Diffusion . . . 21
- 3.4 Creep . . . 22
- 3.5 Deformation Mechanism Map . . . 23
- 3.6 Dominant Deformation Mechanisms . . . 24

4 Models for Plastic Flow of Ti-6Al-4V **25**
4.1 Empirical Models . . . 25
4.1.1 Johnson-Cook Model . . . 25
4.1.2 Sellars-Tegart Model . . . 26
4.1.3 Polynomial Relation Model . . . 27
4.2 Physically Based Models . . . 28
4.2.1 Meyers Model . . . 28
4.2.2 Majorell Model . . . 28
4.2.3 Armstrong Zerilli Model . . . 29
4.2.4 Nemat-Nasser Model . . . 30

5 Dislocation Density Based Model **31**
5.1 Formulation of the model . . . 31
5.2 Bridging Scales . . . 31
5.2.1 Flow Stress . . . 32
5.2.2 Evolution of immobile dislocation density . . . 34
5.2.3 Evolution of excess vacancy concentration . . . 36
5.2.4 Model for Self Diffusion . . . 37
5.2.5 Stress-Update . . . 38
5.3 Optimization of the model . . . 40
5.4 Model and experiments . . . 43

6 Conclusions and Future Work **47**

References **55**

Chapter 1

Introduction

Ti-6Al-4V has good specific strength, toughness and corrosion resistance which makes it attractive for applications in aerospace, pressure vessels, surgical implants etc. Components for these applications have precise requirements on mechanical and physical properties (James and Lutjering, 2003). Besides, this alloy has a narrow temperature and strain rate window of workability (Kailas et al., 1994, Seshacharyulu et al., 2002). Optimization of the process parameters to satisfy the requirements on the component can be enabled by simulation.

The deformation mechanisms of crystalline materials involve various phenomena depending on the temperature, stress levels and strain rates. Chapter 2 explains the active deformation mechanisms in polycrystals. In Chapter 3, the various microstructural changes of Ti-6Al-4V during temperature and mechanical loading are studied. The dominant deformation mechanisms of this alloy are identified to be dislocation glide controlled by Peierls-Nabarro stress and dislocation climb controlled by lattice and core diffusion. Self diffusivity of the alloy is enhanced by the short circuit pipe diffusion at low temperature ($< 0.5T_{melt}$). In Chapter 4, the various flow stress models available in literature for Ti-6Al-4V are reviewed and compared for their capability to model the complex deformation mechanisms.

Chapter 5 explains the adaptation of a physically based constitutive model for 316L Steel formulated by Lindgren et al. (2008) to Ti-6Al-4V. Similar models have been proposed by Nemat-Nasser et al. (1999) for commercially pure Ti and Picu and Majorell (2002) for Ti-6Al-4V with the exception of the effects of vacancy formation and its evolution. This work extends the dislocation density based model (Lindgren et al., 2008) by including the effects of enhanced diffusivity. Additionally, the capacity of the model to simulate diffusion assisted deformation mechanisms responsible for creep and stress relaxation are illustrated in this chapter.

1.1 Background

This work is part of a project aimed to perform finite element simulations of a manufacturing chain involving hot-forming, welding, metal deposition and heat treatment of Ti-6Al-4V components. Manufacturing chain simulations can compute the cumula-

tive effect of the various processes by following the material state through the whole chain and give a realistic prediction of the final component. Capacity to describe material behavior in a wide range of temperatures and strain rates is crucial for this task. The hypothesis in the current work is that such a model should be based on the physics of the material behavior.

1.2 Scope of this work

The scope can be phrased as the following question.

What model, including its parameters can be used to describe the deformation behavior of Ti-6Al-4V during forming, welding and heat treatment processes?

In this thesis, the dominant deformation mechanisms of the alloy are identified from the existing published literature. A suitable physically based model is chosen and calibrated with one dimensional isothermal compression tests. The flow stress is computed based on the evolution of internal state variables like dislocation density and vacancy concentration. The isotropic hardening model used here ignores the anisotropy of the material. This model could predict stress relaxation with an accuracy adequate for simulating heat treatment.

Chapter 2

Deformation Mechanisms of Polycrystals

On application of an external force, crystalline materials undergo deformation. This shape change is reversible or elastic if the applied force produces a small deformation ($\varepsilon < 10^{-4}$). During elastic deformation, the atoms will be displaced from their average positions, but will not change their relative positions. The theoretical shear strength (resistance to move a plane of atoms past another) of a single crystal is approximately $10^{-2}G$ as opposed to (10^{-4}-10^{-8})G for measured resolved shear strength, where G is the shear modulus (Hull and Bacon, 2001). This is because deformation is facilitated by the introduction of dislocations and imperfections in the crystal lattice as shown in figure 2.1. Propagation of dislocations consume lower energy than breaking of atomic bonds along a plane of atoms. Dislocations travel in a preferred direction depending on the crystal orientation and applied force. It is the formation, evolution and interaction of the lattice imperfections that constitute the various deformation mechanisms.

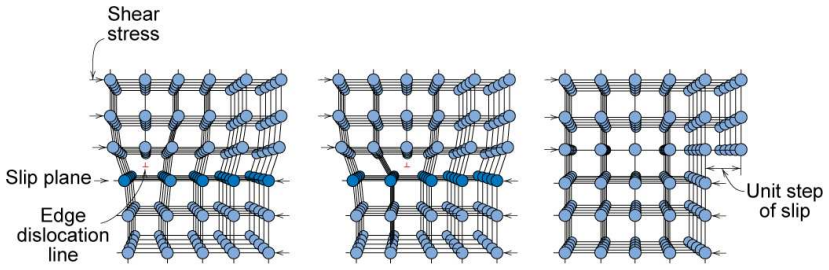

Figure 2.1: Plastic deformation facilitated by propagation of dislocations (William D. Callister, 2006).

2.1 Point Defects

Vacancies and interstitials shown in figure 2.2 are common defects in crystal lattices. These point defects will introduce strains in the lattice. Vacancy is produced when an atom jumps from a lattice position to an interstitial site producing a self interstitial. Both these defects generate equal lattice strain energies. A substitutional impurity is produced when an external atom occupy the lattice position of the material. Its strain energy is the lowest if the atoms are approximately of the same size. Atom of an external material residing in the interstitial location of a crystal produces an interstitial impurity. They are usually smaller in size as compared to the lattice atoms and therefore posses lowest strain energy.

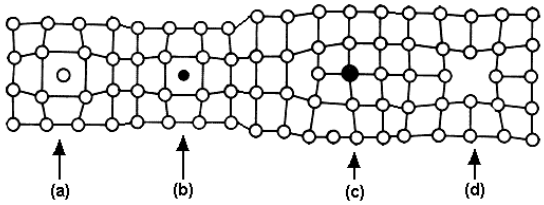

Figure 2.2: a) Self interstitial, b) Interstitial impurity, c) Substitutional, and d) Vacancy.

2.2 Line defects

Edge dislocations are crystalline imperfections constituted by an extra half plane of atoms (see figure 2.1). The terminating line of the extra plane locates the region of severe lattice strain. On application of an external shear force, this plane progressively makes and breaks bonds with the atoms in the lattice. A screw dislocation is an imperfection where one part of the plane moves toward the right and other part moves to the left thereby moving the dislocation normal to the direction of application of force. Figure 2.3 show the motion of edge and screw dislocations.

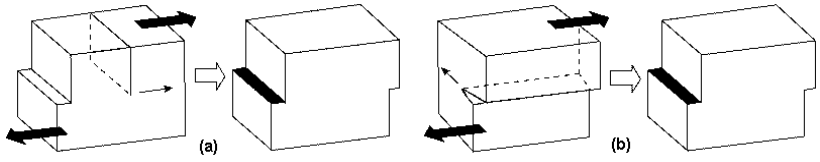

Figure 2.3: a) Edge dislocation and b) Screw dislocation.

2.2.1 Jogs and Kinks

Jogs and kinks are defects in a dislocation which occur frequently in the lattice and strongly affect its mobility. Figure 2.4 shows the jogs and kinks in the lattice. They are defined as steps in a dislocation line of atomic dimensions present in all kinds of dislocations which are formed by a thermally activated mechanism. Kinks fall in the glide plane whereas jogs do not. Both of them can be formed by intersection of dislocations. The movement of a jog by addition and emission of interstitial atoms is shown in figure 2.5

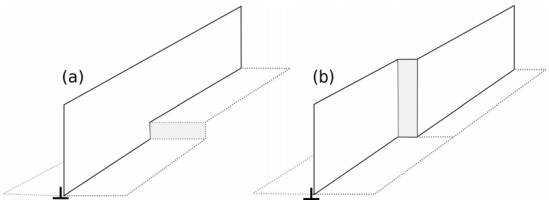

Figure 2.4: a) Jog and b) Kink in edge dislocation.

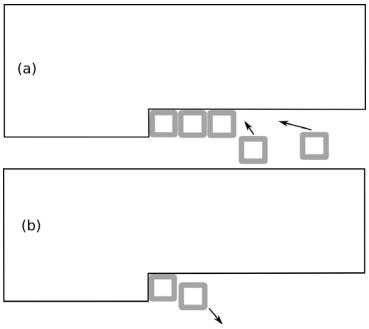

Figure 2.5: a) Movement of jog by addition of interstitials and b) Movement of jog by absorption of vacancies and emission of interstitials.

2.3 Planar defects

Planar boundaries are formed in a lattice due to changes in orientation. They are classified based on the mis-orientations as, Low Angle Grain Boundary (LAGB) and High Angle Grain Boundary (HAGB). Tilt and Twist boundaries belong to the LAGB group with angle of mis-orientation lower than 11° whereas grain and phase boundaries belong to HAGB with a mis-orientation greater than 15° (Humphreys and Hatherly, 2004)(see figure 2.6). Twinning is a low temperature deformation mechanism where a lattice volume upon shear would transform itself into an orientation with mirror symmetry relative to the parent lattice. Twins formed during recrystallization or grain growth are known as annealing twins. Tilt boundaries are formed

when dislocations of the same polarity get aligned. This produces a low energy orientation and splits the parent grain lattice to subgrains. Twist boundaries are similar to tilt boundaries but are twisted in a direction normal to the boundary plane. In reality, tilt and twist boundaries are mixed up. Two different phases or lattice with different orientations that share an interface plane and are oriented with a high angle between them produce a phase or grain boundary.

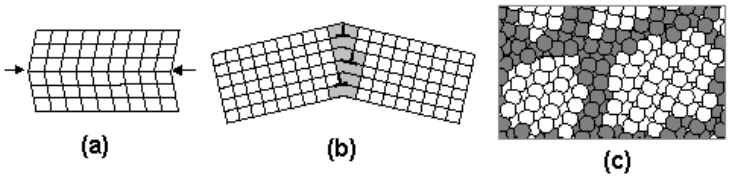

Figure 2.6: a) Twin Boundary, b) Tilt boundary and c) Grain boundary.

2.4 Plasticity

Plastic flow of a material is governed by the motion of dislocations. This is a kinetic process which involves gliding of atomic planes, diffusive flow of atoms, vacancies and interstitials, climb of dislocations normal to glide plane, grain boundary sliding, twinning, etc. These mechanisms vary and overlap with magnitude of stress, strain rate, temperature and microstructure of the material. However, dislocation glide is the dominating factor for plasticity at temperatures less than $0.4T_{Melt}$.

2.4.1 Hardening Process

Moving dislocations when confronted with obstacles produce pileups resulting in a reversed stress which oppose the applied shear stress. This is manifested in the stress-strain curve as hardening behavior. The force necessary for plastic flow is the difference between shear stress and the back stress. All crystalline imperfections act as obstacles to dislocation motion with varying degrees and further escalates the defect formation. Therefore the plastic flow of a material can be controlled by regulating the dislocation motion which can be achieved by introducing or removing crystalline defects. The yield strength of a material depends on long range and short range obstacles created by the imperfections written as (Hertzberg, 1995).

$$\sigma_{yield} = \sigma_{short} + \sigma_{long} + \sigma_{very-long} \tag{2.1}$$

Here, σ_{short} is due to the short range interactions of dislocations to overcome the lattice resistance field of the order less than 10Å. This is strongly temperature sensitive and has additional contributions from point defects. σ_{long} is the temperature independent component that is due to long range interactions of dislocations with substructures of the order $(10^2 - 10^3$Å). Here, dislocation-dislocation, dislocation-precipitate and dislocation-solute interactions are important. $\sigma_{very-long}$ is due to structural size obstacles like planar defects of the order greater than 10^4Å.

2.4.2 Restoration Processes

Plastic deformation changes the microstructure of the material by introducing defects in the lattice. This corresponds to the energy stored (≈10%) by the material as strain energy due to lattice distortions which is the difference between work done for deformation and adiabatic heating (Reed-Hill and Abbaschian, 1991). Every material can store a limited amount of lattice strain energy which reduces with increasing temperature. When in excess, this energy is released, and produces a lattice with lesser defects which is called restoration. During this process, the dislocations which are pinned by obstacles are assisted thermally or by the stored energy to remobilise themselves reducing the flowstrength of the material. Recovery and recrystallization are competing restoration mechanisms driven by the stored energy of the crystal and each of them consist of a series of events. Recovery process shown schematically

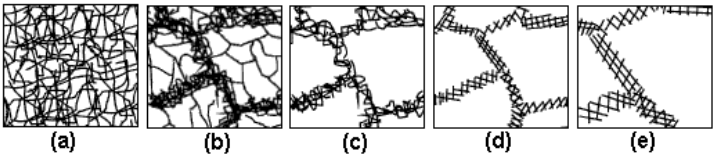

Figure 2.7: a) Pileups, b) Cell formation, c) Annihilation, d) Subgrain formation and e) Grain growth.

in figure 2.7 involves formation of cells, annihilation of dislocations, formation of subgrains and grain growth occurring with some overlap (Humphreys and Hatherly, 2004). Cells are regions of low dislocation density (channels) surrounded by regions with high density of dislocations with alternating polarity (walls). Subgrains are similar to cells except that the walls contain dislocations with same polarity and are neatly arranged. Recovery during deformation is known as Dynamic Recovery (DRy) and after deformation is Static Recovery (SRy). Recovery produces subtle changes in the microstructure that cannot be observed by an optical microscope, but brings in large changes in mechanical property; *viz* yield strength, hardness etc. This can be quantitatively measured by using Differential Scanning Calorimetry (DSC) or hardness measurements (Knudsen et al., 2008, Woldt and Jensen, 1995). The rearrangement of dislocations to form low energy structures is called polygonisation or cell formation. Based on the Read-Schockley equation (Read and Shockley, 1950), energy of a tilt boundary increases with increasing mis-orientation and energy per dislocation decreases with increasing mis-orientation. This indicates that a fewer highly mis-oriented boundaries are favored after recovery. The glide and climb of dislocations allow dislocations to move and reorganize. This also results in the annihilation of dislocations with opposite polarity.

Glide

Thermally activated glide or cross-slip has been accounted for as a recovery mechanism (Fridel, 1964). During cross-slip, dislocations move along the plane driven by applied stress or stored energy. Dislocations try to rearrange themselves and possibly annihilate or exit through the free surface in order to produce a low energy state

by distorting the lattice. Figure 2.8 show the glide of edge and screw dislocations. Various obstacles like precipitates, solutes, immobile dislocations etc are responsible for inducing a glide resistance which may vanish or rearrange during restoration processes (Kocks et al., 1975).

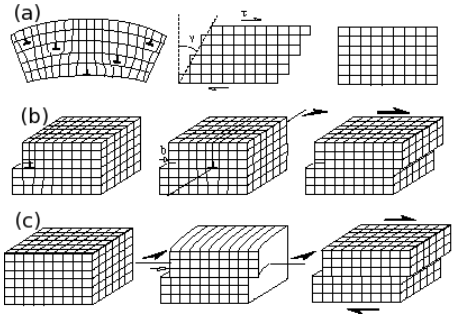

Figure 2.8: a)Recovery of dislocations by glide, b)Glide of edge dislocations and c)Glide of screw dislocations.

Climb

Climb is a thermally activated mechanism driven by vacancy motion due to lattice diffusion and jogs which enables dislocations to circumvent obstacles (see figure 2.9). At elevated temperatures, activation energy for formation and motion of vacancy otherwise known as activation energy for self diffusion is the controlling factor. At low temperatures, the activation energy for formation of jog contributes to the activation energy for self diffusion. In some cases, the diffusion along dislocations (core diffusion) can be the controlling factor for climb as the activation energy for core diffusion is lower than for self diffusion (Cahn and Peter, 1996b, Humphreys and Hatherly, 2004, Prinz et al., 1982).

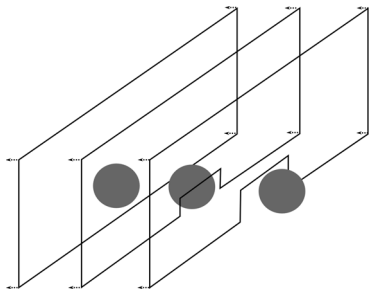

Figure 2.9: Dislocations climbing past an obstacle.

Recrystallization

Recrystallization (Rx) is the nucleation and growth of new grains with fewer defects at regions of high energy gradient. These grains will consume the deformed microstructure as it grows. During deformation, the amount of stored energy is increased by the presence of multiple phases and precipitates where large particles will act as sites of nucleation. They can also hinder grain growth by pinning the grain boundaries (Humphreys and Hatherly, 2004). Rx occurs in different time scales. A low temperature deformed material subjected to elevated temperature can result in Rx known as Static Recrystallization (SRx). Dynamic Recrystallization (DRx) can be considered as the SRx occurring in the time scale of deformation (Barnett et al., 2000).

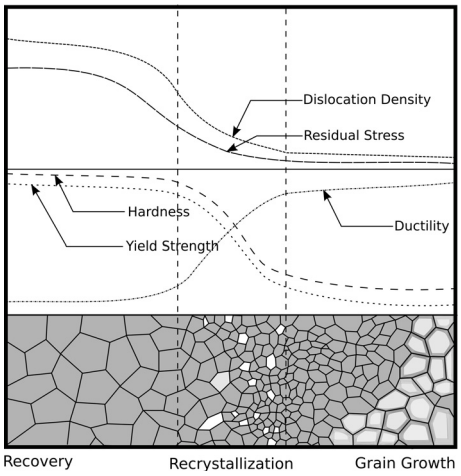

Figure 2.10: Restoration processes.

Some materials can store a high amount of energy even at elevated temperatures. This is primarily due to the slow recovery process which favors DRx. For DRx to occur, the driving force or defect energy present in the deformed microstructure must be high enough. This requires the temperature to be sufficiently low to ensure storing of adequate energy and high enough to provide the needed activation energy. During Rx, the density of dislocations and thereby the fraction of LAGB is reduced by a diffusion process. The mechanism of grain boundary migration in LAGB is by the climb of individual dislocations, whereas in HAGB, it is one of atomic jumps across boundaries. In the intermediate ranges its more difficult and vague (Humphreys and Hatherly, 2004). Figure 2.10 shows the response of the material to various restoration processes. The hardness, yield strength and dislocation density drop suddenly at the same rate during recrystallization while the residual stress undergoes a more gradual reduction during recovery and gets saturated during recrystallization. The ductility of the material increases during recrystallization and gets saturated during grain growth.

2.5 Creep

Most materials at elevated temperature when applied with a constant stress, undergo a transient response with a reducing strain rate ($\dot{\varepsilon}$) towards a constant value which lasts for a long time. Later the $\dot{\varepsilon}$ increases rapidly leading to rupture. These three regions shown in figure 2.11 can be attributed to different deformation mechanisms. Primary creep is due to substructure changes and leads to dislocation hardening. The stable secondary creep is due to the dynamic balance between hardening and restoration. However, the final unstable tertiary creep can be due to metallurgical instabilities like corrosion, granular shear, granular fracture, cavitation, necking, dissolution of precipitates etc. A material which undergoes creep might also exhibit

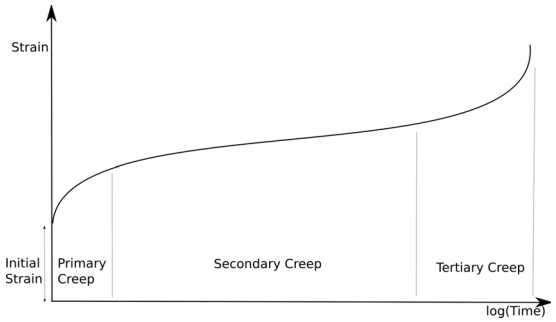

Figure 2.11: Creep curve.

strain recovery and stress relaxation as shown in figure 2.12 (Stouffer and Dame, 1996). On removal of creep stress, the material undergoes instantaneous elastic recovery followed by a slow recovery phase. The driving force for this process is the stored energy during creep deformation. Stress relaxation is the decay of stress with time while a material is held at a constant nonzero strain. Depending on the stress and temperature, the possible creep mechanisms can be dislocation creep, dislocation glide, bulk diffusion, grain boundary diffusion, granular shear, granular fracture, etc.

2.5.1 Dislocation Creep

The motion of dislocations during creep is believed to be controlled by self diffusion because of the similarity in the activation energy. Vacancies assist the motion of dislocations to overcome obstacles on their slip planes. It requires the combined effect of a group of vacancies for a dislocation line to climb. The probability of climb at elevated temperature is increased largely because of the high equilibrium vacancy concentration.

When the vacancies get closer to dislocation core, they replace atoms in the core and dislocations move perpendicular to the glide plane on to the nearest neighboring plane (Gottstein, 2004). In many materials, climb of dislocations is controlled by core or pipe diffusion rather than by lattice diffusion (Humphreys and Hatherly, 2004).

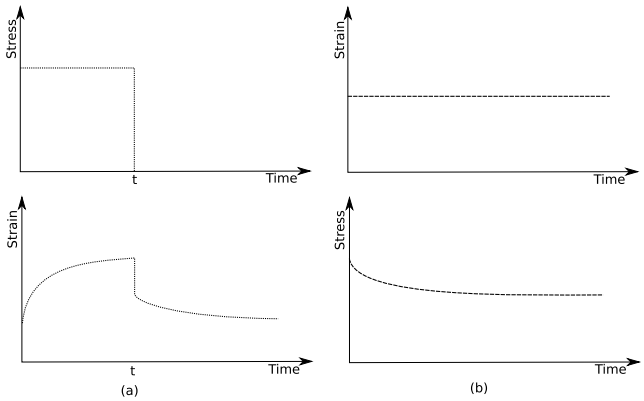

Figure 2.12: a) Creep followed by recovery and b) Stress relaxation test.

2.5.2 Nabarro-Herring Creep

At high temperature and low stress, creep occurs not by motion of dislocations, but by the transport of matter through volume diffusion as shown in figure 2.13(a). This is driven by the chemical potential of atoms which depend on the elastic stress state leading to motion of atoms from a compressed region to a dilated region. The strain rate is equivalent to the diffusive motion of the atoms which is proportional to the applied stress.

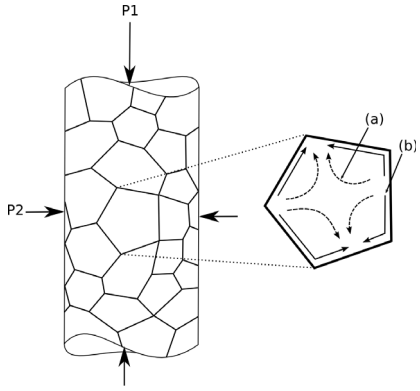

Figure 2.13: a) Nabarro-Herring creep and b) Coble creep.

2.5.3 Coble Creep

At a lower temperature, fine grained materials allow transport of material along its grain boundaries as shown in figure 2.13(b). This flow which is limited to grain boundary can be much higher than the volume diffusion.

Both Nabarro-Herring and Coble creep occur in polycrystals. But it is less prominent in metals as compared to ceramics because the dislocation creep is the dominant mechanism in metals. Grain boundary strengthening can deteriorate creep resistance of a material because it enhances the diffusivity.

2.5.4 Granular Shear

The motion of grain boundaries relative to each other as shown in figure 2.14 is known as grain boundary shear. The direction of shear is the boundary lying along the direction of critical resolved shear stress. This is also known as grain boundary sliding and can lead to spasmodic and irregular flow of material.

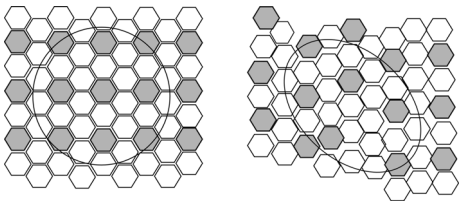

Figure 2.14: Motion of grain boundaries along its boundaries.

2.5.5 Granular Fracture

At temperatures below $0.5T_{Melt}$, metals may fail by transcrystalline fracture that occurs as a secondary stage of grain boundary shearing. This often results in formation of cavities in the corners of grains or pores along the grain boundaries. The former is produced by higher creep rate and stress while the latter by lower strain rate and stress. Fracture occurs when the stress concentration exceeds the cohesive strength of the grain boundaries (see figure 2.15). Plastic flow, grain boundary sliding and grain boundary migration can act as a hindrance for granular fracture.

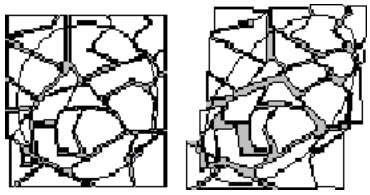

Figure 2.15: Intercrystalline fracture.

Chapter 3

Ti-6Al-4V Microstructure and Properties

Ti-6Al-4V is a two phase ($\alpha + \beta$) alloy with a variety of possible microstructures. The proportion of Al and V gives attractive mechanical properties to the material. Ti-6Al-4V contains 6wt% Al stabilizing the α-phase which has HCP structure and 4wt% V stabilizing the β-phase which has BCC structure. The two phases have different properties given by their structures, with α exhibiting greater strength yet lower ductility and formability (Tiley, 2002). The microstructure at equilibrium and in room temperature consists mainly of α-phase ($\approx$95%) with some retained β-phase.

The various physical properties of this alloy are dependent on factors such as thermo-mechanical processing, chemical composition and interstitial impurities, mainly oxygen (Odenberger, 2005). The common heat treatments employed for Ti-6Al-4V are mill annealing, duplex annealing and solution treatment (Donachie, 1988). Mill annealing is achieved by keeping the specimen at 720 °C for about an hour, followed by slow cooling. This will result in a microstructure of globular β in an α matrix which is soft and machinable. β-annealing or duplex annealing is achieved by 30min annealing at 1030 °C, followed by air cooling and 2h ageing at 730 °C. Solution treating or α+β field annealing consist of keeping the material at 950 °C for 10min followed by 4h annealing around 600 °C and air cooling. Table 3.1 shows the variation of mechanical properties with heat treatment. If properly processed, this alloy can have better strength than α or β alloys (Donachie, 1988). Commercial

Table 3.1: Effect of processing on material property.

Heat treatment	Yield strength (MPa)	Elongation (%)
Mill Annealed	945	10
Duplex Annealed	917	18
Solution Treated	1103	13

Purity (CP) Ti-6Al-4V contains (0.16-0.18) wt% oxygen whereas Extra Low Interstitial (ELI) Ti-6Al-4V contains (0.1-0.13) wt% oxygen. ELI Ti-6Al-4V has lower room temperature strength than CP Ti-6Al-4V whereas the later has lower elongation and fatigue life (Tiley, 2002). Low-temperature plasticity in α-Ti is extremely sensitive to the concentration of the interstitial impurities.

The morphology of Ti-6Al-4V can be classified as lamellar, equiaxed and a mixture of both. The lamellar structure can be controlled by heat treatment. The cooling rate from above the β-transus temperature determines the size of the lamellas. Higher cooling rate imply finer lamellas. The equiaxed microstructures can be obtained by extensive mechanical working in the $(\alpha + \beta)$ phase region during which, the lamellar α breaks up into equiaxed α. The bimodal type of microstructure is obtained by annealing for 1hr at 995 °C followed by cooling and aging at 600 °C. The result is a structure consisting of isolated primary α grains in a transformed β matrix (Westman, 2003).

3.1 Phase Evolution

The temperature at which α changes to β (β-transus) depends on the composition of Al and V (see figure 3.1). The β-transus is also sensitive to interstitial impurity; for example, higher amount of oxygen will raise β transus , whereas higher amounts of Fe will lower it (Prasad et al., 2001). Depending on the processing conditions, this alloy can form two stable phases (α and β), two metastable phases ($\alpha\prime$ and $\alpha\prime\prime$) and the intermetallic phase α_2

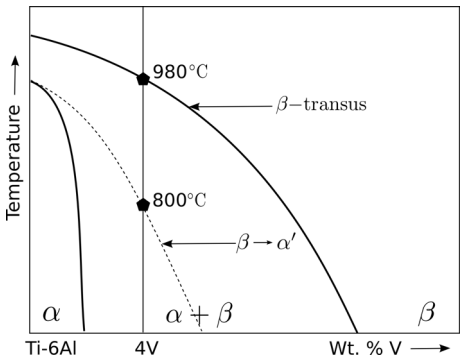

Figure 3.1: Ternary phase diagram.

3.1.1 The Primary phases (α, β)

When cooled from β-transus temperature (980 °C), the HCP α-phase starts to form as plates with basal plane parallel to a special plane in β-phase. The growth is fast along the plates as compared to the perpendicular direction. Later, this develops to parallel α plates with β trapped between them. Also, the plates formed parallel to one plane of β will meet plates formed with another plane which is demonstrated schematically in

figure 3.2. This process is referred to as 'sympathetic nucleation and growth' which results in a structure commonly known as 'Widmanstätten' (James and Lutjering, 2003). The kinetics of beta to alpha transformation has been studied by Malinov

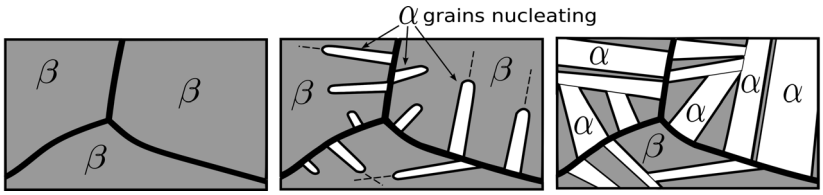

Figure 3.2: Formation of Widmanstätten structure.

et al. (2001) using DSC at continuous cooling conditions with constant cooling rates. This phenomenon was modelled using the Johnson-Mehl-Avrami equation. Figure 3.3 shows the predictions of their model. The V-enriched BCC β-phase is present in limited quantity in Ti-6Al-4V at room temperature. This phase plays a minor role in strengthening because of its small proportion. As discussed by Picu and Majorell (2002), the mechanical behavior changes remarkably only when the amount of β becomes larger than 50%. The microstructure is composed entirely of β above 980 °C.

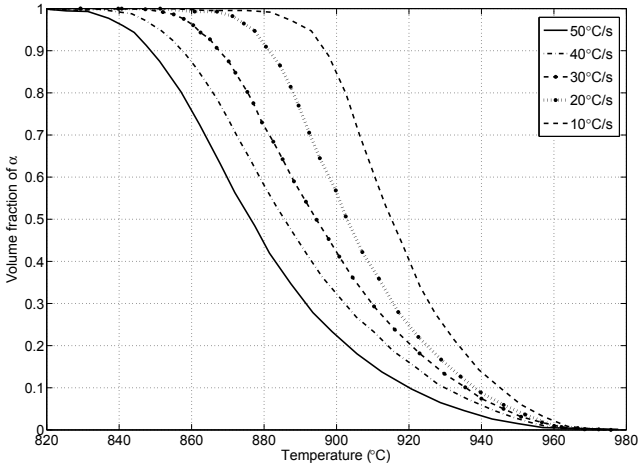

Figure 3.3: α phase fraction evolving with temperature.

3.1.2 The metastable phases ($\alpha\prime$, $\alpha\prime\prime$)

The physical and mechanical properties of Ti-6Al-4V are very much influenced by the presence of metastable phases which are formed during rapid cooling. One such phase is $\alpha\prime$ (see figure 3.1 for its formation temperature) which has HCP structure and due

to its rapid nucleation and growth contains a higher dislocation density compared to the primary α grains. Hence, the deformation mechanisms in $\alpha\prime$ are similar to those in α, with the main difference being a higher dislocation density in the undeformed state and a smaller plate thickness. Both the smaller grain size and the higher dislocation density suggest that $\alpha\prime$ is harder than α. Also, this phase can undergo more strain hardening than α phase. Another metastable phase in Ti-6Al-4V is the $\alpha\prime\prime$ with a rhombic structure instead of hexagonal (Moiseyev, 2005). This can be considered as an intermediate between HCP and BCC with the mechanical properties close to that of the α phase.

3.1.3 The Intermetalic phase (α_2)

During heating of Ti-6Al-4V above 500 °C, alloy element partitioning takes place leaving a larger % fraction of elements like Al, O and Sn available for enriching the alpha phase. This leads to the precipitation of the coherent Ti_3-Al particles which is also known as α_2 phase. These particles can be sheared by dislocations and also can have extensive pileup of dislocations against boundaries (James and Lutjering, 2003). Ti_3-Al particles grow in ellipsoidal shape with its long axis parallel to the c-axis of the hexagonal lattice. The presence of O and Sn can further enhance the precipitation of this intermetallic phase.

3.2 Plastic flow

Plastic flow of Ti-6Al-4V subjected to a wide range of temperatures and strain rates have been reported in literature (Barnett et al., 2000, Bruschi et al., 2004, Ding and Guo, 2004, Ding et al., 2002, Fujii and Suzuki, 1990, Johnson et al., 2003a,b, Kailas et al., 1994, Khan et al., 2007, Li, 2000, Montheillet, 2002, Mosher and Dawson, 1996, Nemat-Nasser et al., 2001, Nicolaou et al., 2005, Park et al., 2002, Prasad and Seshacharyulu, 1998, Semiatin and Bieler, 2001, Semiatin et al., 1998, 1999, Sheppard and Norley, 1988, Vanderhasten et al., 2007). The flow curves obtained from compression testing in the range of temperatures from 20 °C to 1000 °C, and strain rates from $10^{-3}s^{-1}$ to $1s^{-1}$ are given in figures 3.4, 3.5 and 3.6. The compression tests performed at 20 °C to 500 °C resulted in hardening followed by fracture and at temperatures between 600 °C to 900 °C resulted in flow softening after the initial hardening (see figure 3.5). It can be noted that at temperatures nearing to 1000 °C, the material behavior is close to elastic perfectly plastic (see figure 3.6). Since the flow curves are smooth and do not exhibit serrations, the presence of dynamic strain ageing can be ruled out. Figure 3.7 shows the temperature dependant youngs modulus and thermal strain. The youngs modulus is obtained from isothermal tension tests and the thermal strain is measured using a differential expansion dilatometer.

3.2.1 Strain rate sensitivity

At temperatures below room temperature, the temperature sensitivity is dependent on the Al concentration. This effect can be modelled by considering the Peierls stress to be dependent on the Al concentration, or by defining an equivalent Peierls stress. Additionally, the activation energy for self-diffusion of Ti in the α-phase is similar to

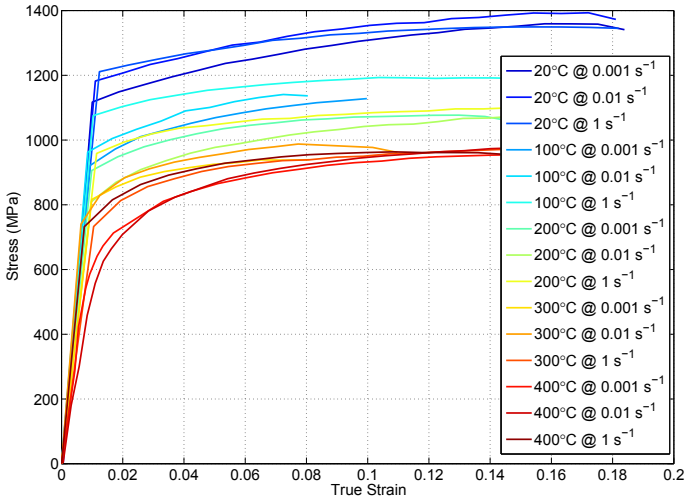

Figure 3.4: Flow curves from hot compression tests between 20 °C to 400 °C.

that for self-diffusion of substitutional Al in Ti-6Al-4V. From this, it can be concluded that deformation in this temperature regime is controlled by the thermal activation of dislocations over short-range obstacles (Chichili et al., 1998).

From figure 3.8, it can be seen that the material is almost strain rate insensitive at lower temperature and sensitivity increases rapidly towards the β-transus temperature. According to Majorell et al. (2002), the increase in strain rate sensitivity in the high temperature range can be attributed to its large grain size. Grain boundary sliding close to the β-transus can also lead to the increase in strain rate sensitivity. Nemat-Nasser et al. (2001) studied the dependence of flow stress on temperature and strain rate for various strains and material microstructure. Adiabatic shear bands were observed during high and low strain rates as well as at high temperatures. The flow stress is more sensitive to temperature than to strain rate. Based on this results and other supporting literature, they have identified the thermally activated mechanisms for dislocation motion.

3.2.2 Hall-Petch Relation

The HCP structure has limited independent slip systems and this lead to high grain boundary strengthening.the Hall-Petch relation is valid also in two phase $\alpha + \beta$ titanium alloys with Widmanstatten or colony alpha microstructures. Since the α phase is much stronger compared to β, it can be assumed that the phenomena related to grain boundary strengthening is occurring only inside the α phase and the β phase can be considered as a grain boundary (Semiatin and Bieler, 2001). The flow stress of Ti-6Al-4V is independent of colony size at temperatures between 815 °C and 955 °C. This suggests that plastic flow is controlled by glide and climb of dislocations at these temperatures.

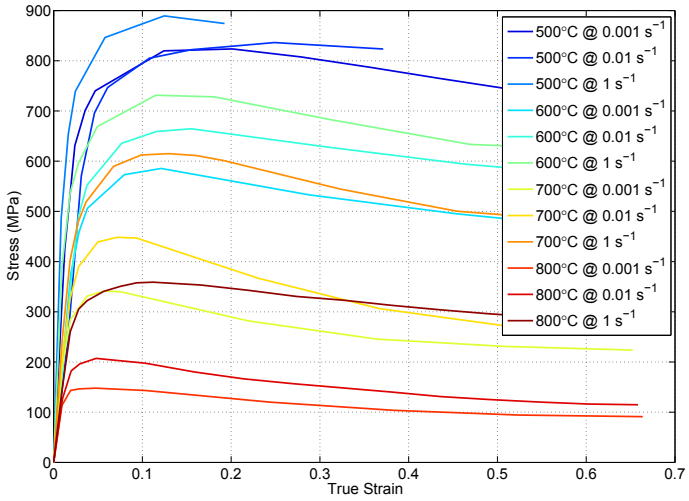

Figure 3.5: Flow curves from hot compression tests between 500 °C to 800 °C.

3.2.3 Twinning

Twinning is an important deformation mechanism in HCP materials. Un-alloyed Ti loaded at low strain rates twins at all temperatures below 500 °C (Chichili et al., 1998). At higher temperatures it twins only under high strain rate loading. Presence of Al inhibits twinning so that Ti-6wt% Al does not twin even at very low temperatures. Therefore twinning is not a major deformation mechanism in Ti-6Al-4V at all rates and temperatures of practical interest.

3.2.4 Flow Softening

Flow softening (reduction of resistance to plastic flow) is observed during compression tests at temperatures between 500 °C and 800 °C in Ti-6Al-4V. This can be attributed to adiabatic heating, dynamic microstructural changes, localisation etc. Deformation heating can be ruled out in this case because of the low strain rates applied. Microstructural changes include change in volume fraction of the phases, morphology change, substructure change, recrystallisation, etc. Localisation denotes shear band formation and damage.

Recrystallisation

The deformation characteristics of Ti-6Al-4V during torsion in the temperature range (800-1150) °C have been studied by Sheppard and Norley (1988). Based on optical and electron microscopy studies, they have established that dynamic recovery is the operative deformation mechanisms in the β-region, while DRx predominates in the $\alpha + \beta$ region. Majorell et al. (2002) observed no significant recrystallisation in Ti-6Al-4V during forging in the $\alpha + \beta$ domain, particularly when the forging operation is followed by quenching. Limited recrystallisation is observed even inside deformed

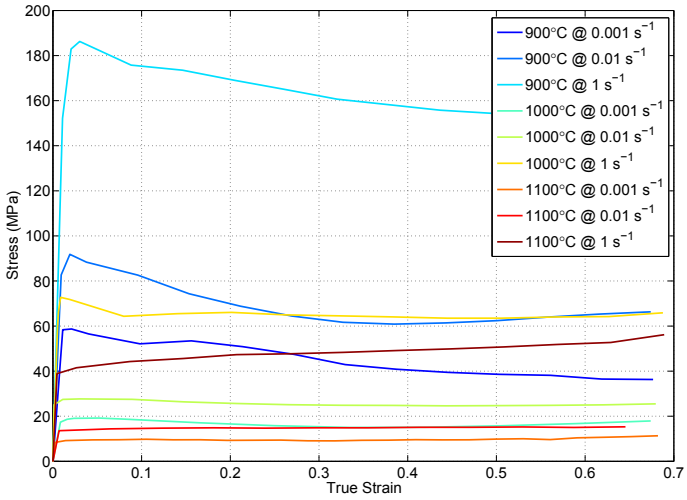

Figure 3.6: Flow curves from hot compression tests between 900 °C to 1100 °C.

adiabatic shear bands where the total strain, the strain rate and temperature are much higher than usually encountered in a homogeneous test.

Deformation of Ti-6Al-4V at a strain rate of $5 \cdot 10^{-4}\text{s}^{-1}$ from room temperature to 1050 °C has been studied by Vanderhasten et al. (2007). Using microstructural, EBSD and mechanical investigations, they observed that from 650 °C to 750 °C, grain boundary sliding is the dominant mechanism. Between 750 °C and 950 °C, DRx and grain growth occur that result in superplasticity and at higher temperatures, it is only grain growth.

Globularisation

Grain growth is usually observed during superplastic deformation of this material. In specimens with larger grains tested under conditions described by Picu and Majorell (2002), superplasticity does not occur and a negligible amount of grain growth is observed. Grain boundary sliding occurs in all specimens at high temperatures. This phenomenon is reflected in the much larger activation energy of the deformation than that for self-diffusion (Meier and Mukherjee, 1990). Stefansson et al. (2002) studied the kinetics of static globularisation of Ti-6Al-4V at temperatures between 900 °C to 955 °C and concluded that deformation induced substructure has limited influence on the static globularisation process. The mechanisms of globularisation are studied by Stefansson et al. (2002) and they identified that recovery induced substructure in α-phase and α-β interface energy can affect the rate of globularisation. This pheomenon was modelled using analatical and numerical techniques by Semiatin et al. (2005)

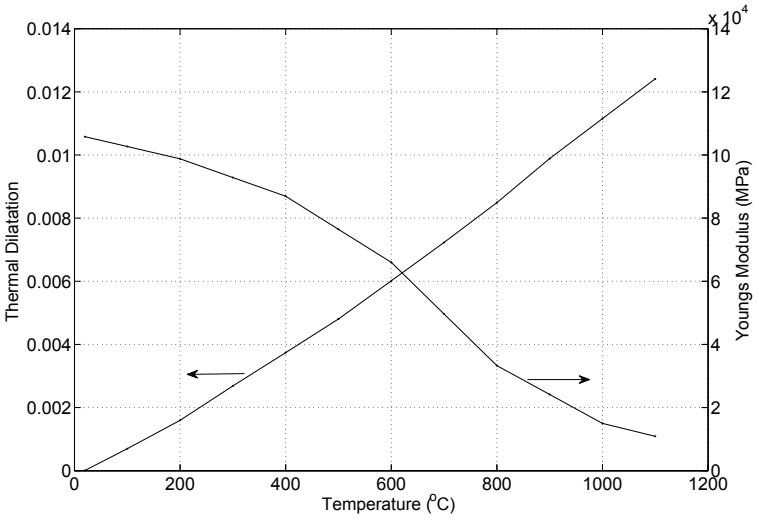

Figure 3.7: Thermal dilatation and Youngs modulus.

3.2.5 Localisation

Concentration of defects in regions of highest principal strain lead to localisation. The specimens fractured catastrophically during the compression tests at temperatures between 20 °C to 500 °C, and at strain rates between $10^{-3}s^{-1}$ to $1s^{-1}$. This can be attributed to shear banding and cavity nucleation which is common for most metals deformed at low temperature.

Shear Banding

Kailas et al. (1994) have studied the failure mechanism of Ti-6Al-4V at low temperatures and strain rates. They have attributed this to adiabatic shear banding and classified the instabilities as 'geometric' as opposed to 'intrinsic' and therefore independent of the dynamic constitutive behavior. Fujii and Suzuki (1990) have observed strain localization at soft β regions close to grain boundary α which is formed at the roots of α side plates near the grain boundary alpha. This is assisted by the presence of β stabilizing elements.

Cavitation

Nicolaou et al. (2005) observed that during torsional loading of Ti-6Al-4V specimens with colony microstructure, cavities appeared along prior-β grain boundaries and triple points. The concentration of cavities was higher along the boundaries perpendicular to the direction of the loading. The cavities grew in an elliptical manner and there were evidences of dynamic globularisation of colony microstructure in the vicinity of the cavity. The effect of local crystallographic texture on the size of cavities

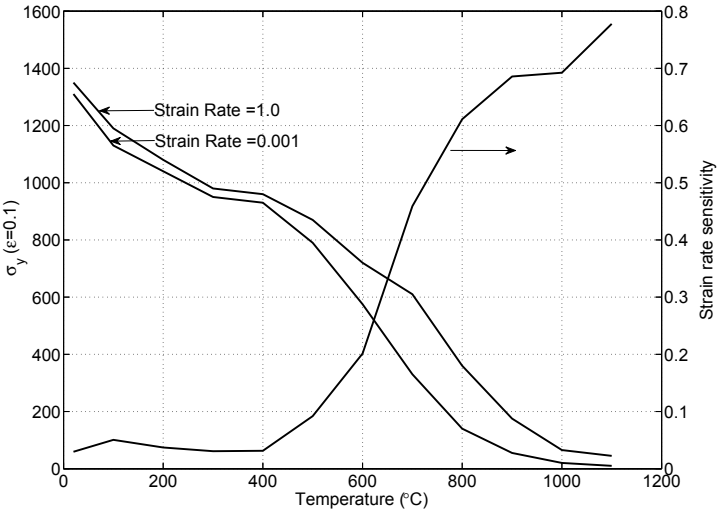

Figure 3.8: Strain rate sensitivity and temperature dependence of flow stress.

formed during hot tension tests for colony microstructure was studied by Thomas et al. (2005). Cavity growth was found to be most rapid at location where (20-40)% of the area surrounding the cavity also had colonies with soft orientations.

Semiatin et al. (1998) studied the kinetics of cavitation during hot tension tests of Ti-6Al-4V at strain rates from $10^{-2}\mathrm{s}^{-1}$ to $3\mathrm{s}^{-1}$. The cavity growth rate was measured to be exponentially increasing with strain. But at temperature close to β-transus, the alloy exhibited ductile rupture with no evidence of cavitation. With decreasing temperature, the cavities grew at the expense of ductility.

3.3 Diffusion

The mechanism of diffusion in Ti systems is less understood and the published diffusion data shows large scatter which is attributed to the variation in measurement techniques (Liu and Welsch, 1988, Mishin and Herzig, 2000). Figure 3.9 shows measurement of self diffusion in α and β Ti by Mishin and Herzig (2000) and the measurement by Semiatin et al. (2003) for Al diffusion in β phase of Ti-6Al-4V. Lattice diffusion is responsible for dislocation climb at high temperatures. However, at intermediate temperatures diffusion along dislocation lines referred to as core or pipe diffusion has a larger effect on climb (Prinz et al., 1982). It has been reported that dislocations in Ti-6Al-4V act as high diffusivity paths leading to an enhanced diffusion (Park et al., 2008). While studying the static grain growth of fine grained Ti-6Al-4V ($g < 2\mu m$), Johnson et al. (1998) has concluded that grain boundary and pipe diffusion are the controlling mechanisms at temperatures less than $0.5T_{melt}$.

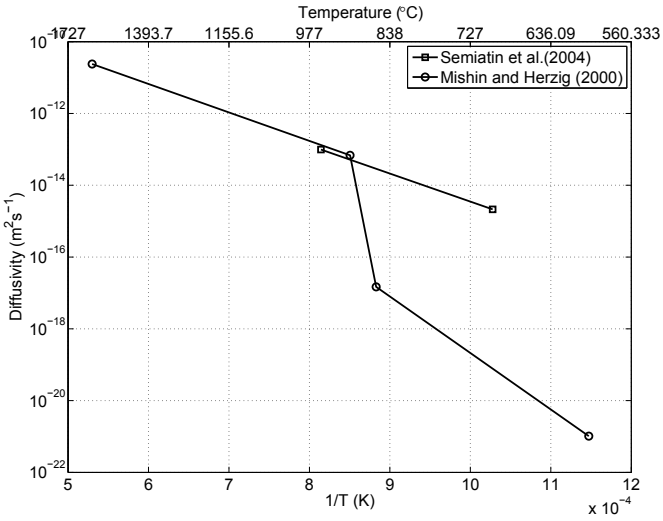

Figure 3.9: Measurements of diffusion.

3.4 Creep

Barboza et al. (2006) studied the creep behavior of the Ti–6Al–4V with a Widmanstätten microstructure under constant tensile loads. They have observed that creep strain rate of Ti–6Al–4V alloy is lower than that of elemental Ti. The creep resistance of Ti–6Al–4V has been attributed to α-β interfaces acting as obstacles to dislocation motion and to the large grain size. Increase of grain size reduces the grain boundary sliding, number of sources for dislocations and the rate of oxygen diffusion along grain boundaries. The increase in tertiary creep rate is related to nucleation and coalescence of microvoids which result in necking. The activation energy for creep in β-Ti is close to that for self-diffusion and therefore can be assumed to be a diffusive transport mechanism (Frost and Ashby, 1982).

The creep failure mechanisms of Ti–6Al–4V alloy in various heat treating conditions have been investigated by Seco and Irisarri (2001). Mill annealed specimens showed the lowest creep resistance and its metallographic analysis revealed that the temperature-activated dislocation climb is the mechanism responsible for failure. The observed voids were generated by plastic deformation, rather than by creep cavitations. β-annealed specimens demonstrated the highest creep resistance. The fracture surfaces of these broken specimens exhibited an intergranular morphology that was attributed to grain boundary sliding along the former beta grains. $\alpha+\beta$ field annealed samples underwent diffusional creep by nucleation and coalescence of the creep cavities generated at the alpha–beta interfaces and the triple points.

3.5 Deformation Mechanism Map

Deformation mechanisms map is a three dimensional representation of the dominant deformation mechanisms of a material subjected to a range of temperatures and stresses (Frost and Ashby, 1982). The three dimensions of the map are normalised stress (σ/G), normalised temperature (T/T_{melt}) and strain rate. Figure 3.10 shows the deformation mechanism map of Ti-6Al with a grain size of 100μm computed by Janghorban and Esmaeili (1991). The the dotted lines indicate the various strain rate contours which passes through different domains of dominant deformation mechanisms as the temperature and stress changes. These net strain rate values are computed by appropriate superposition of all the dominant mecahnisms produced by the combination of given temperature and stress.

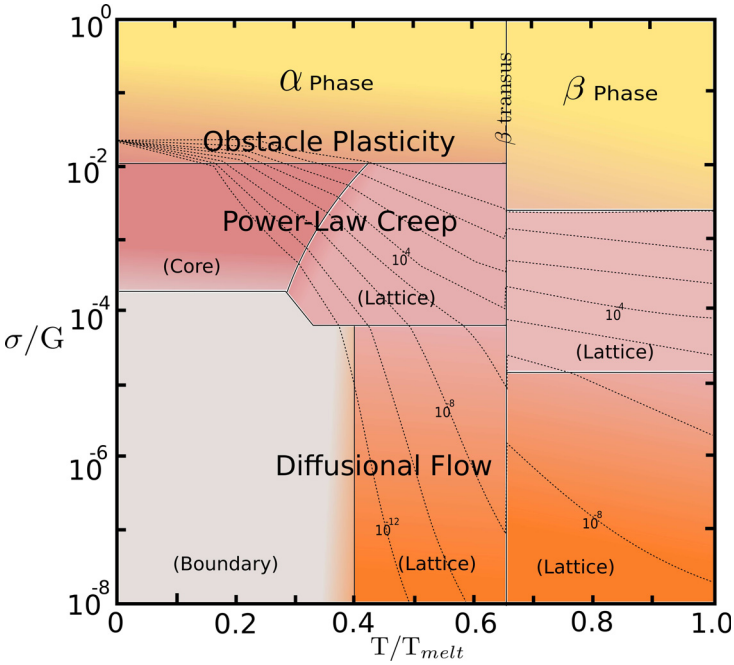

Figure 3.10: Deformation mechanism map.

Prasad and Sasidhara (1997) developed the processing maps based on the estimation of energy dissipation in the microstructure. This stored energy is compared with an ideal linear dissipator to compute the efficiency and stability of the process. Based on processing maps, and microstructural examination of lamellar Ti-6Al-4V, Seshacharyulu et al. (2002) created a variant of the deformation mechanism map which is shown in figure 3.11. This captures most of the phenomena reported earlier in this chapter.

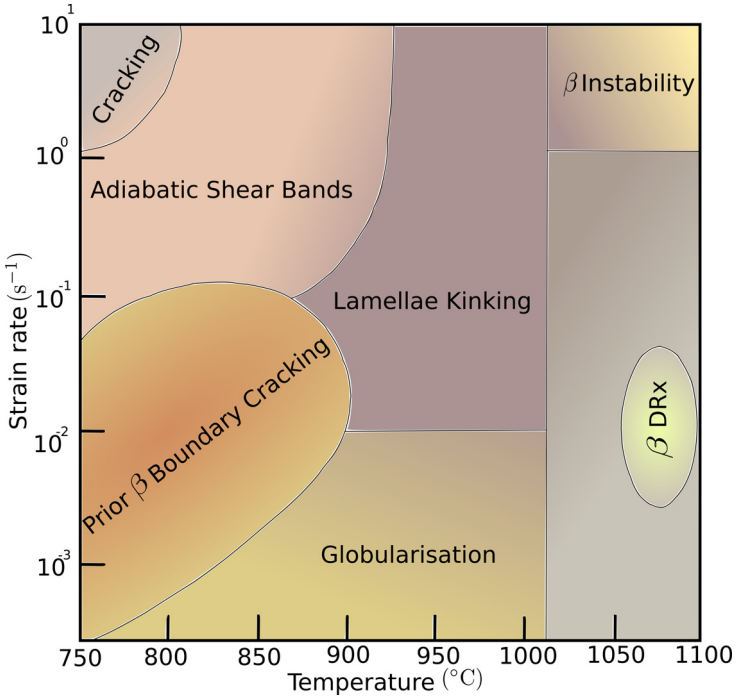

Figure 3.11: Microstructural deformation mechanism map.

3.6 Dominant Deformation Mechanisms

The scope of this work is limited to the strain rates between 10^{-3}s^{-1} to 1s^{-1} and temperature between 20 °C to 1100 °C. Here, at lower temperature, interstitial solutes concentration (C_s) control the plastic flow whereas at higher temperature, it is the concentration of interstitial impurities (C_i) that has control (Conrad, 1981). Studying the effect of strain (ε), strain rate ($\dot{\varepsilon}$), temperature (T) and grain size (g) on Ti systems, Conrad arrived at the following additive strengthening relationship.

$$\sigma = \sigma_G(G, \varepsilon, g, C_s) + \sigma^*(T, \dot{\varepsilon}, C_i) \tag{3.1}$$

Here, first component varies with temperature through the temperature dependence of the shear modulus (G). The second component is strain rate dependent and has short range infulence. The underlying mechanism of plastic flow is identified as dislocation motion by glide and climb which is assisted by diffusion (Conrad, 1981).

Chapter 4

Models for Plastic Flow of Ti-6Al-4V

Engineering or empirical models are determined by means of fitting model equations and parameters with experimental data without considering the physical processes causing the observed behavior. This kind of modeling approach is more common in engineering applications and therefore got the name (Domkin, 2005).

Physically based material models, on the other hand, are models where knowledge about the underlying physical process, dislocation processes etc, is used to formulate the constitutive equations. Naturally, the division between these kinds of models is somewhat arbitrary. Both types of models can be considered "engineering". Developing a physically based model requires more experiments and analysis in different scales as compared to empirical models.

Despite their good fit to the measured stress-strain curves within certain range of strains, strain rates and temperatures, empirical relations have little predictive power beyond that range of deformation conditions and material microstructure used for their calibration. The tabulated data approach has the same limitations as extrapolation is not recommended outside the range of the experimental data.

4.1 Empirical Models

Empirical models like Johnson-Cook, Sellars-Tegart and Polynomial are used to simulate the mechanical constitutive behavior of Ti-6Al-4V by different researchers.

4.1.1 Johnson-Cook Model

Johnson and Cook (1985) model has been widely used to model the high strain rate deformation of metals. The yield stress can be written as

$$Y = (A + B\varepsilon^n)(1 + C \ln \dot{\varepsilon}')(1 - (T')^m) \tag{4.1}$$

where, A is the quasi-static yield strength of the material, ε is the equivalent plastic strain and $\dot{\varepsilon}'$ is non-dimensionalised strain rate. T' is the non-dimensional tempera-

ture calculated by

$$T' = \frac{T - T_{room}}{T_{melt} - T_{room}} \tag{4.2}$$

Temperature change from adiabatic heating can be computed by

$$\Delta T = \frac{\alpha}{\rho C_p} \int \sigma \varepsilon d\varepsilon \tag{4.3}$$

where, α is the percentage of plastic work converted to heat, ρ is the mass density of the material and C_p is the specific heat of the material. Fracture is computed using cumulative damage law (Lesuer, 2000)

$$D = \Sigma \frac{\Delta \varepsilon}{\varepsilon_f} \tag{4.4}$$

where the failure strain is computed as

$$\varepsilon_f = [D_1 + D_2 \exp D_3 \sigma'][1 + D_4 \ln \dot{\varepsilon}'][1 + D_5 T'] \tag{4.5}$$

Here $\Delta\varepsilon$ is the increment of plastic strain in a load increment, σ' is the mean stress normalized by the effective stress and D_1, D_2, D_3, D_4, D_5 are constants. Failure occurs when $D = 1$. The parameters of the model are given in table 4.1.

Table 4.1: Material parameters estimated.

Ref.	A MPa	B MPa	n 10^{-2}	C 10^{-4}	M 10^{-1}	D_1 10^{-2}	D_2 10^{-1}	D_3 10^{-1}	D_4 10^{-3}	D_5 10^{-2}
[a]	Not Published									
[b]	724.7	683.1	47	350	10					
[c]	896	656	50	128	8					
[d]	862	331	34	120	8	-9	2.5	-5	-14	387
[e]	1098	1092	93	140	11	-9	2.5	-5	-14	387

A modified version of Johnson-Cook model is used for Ti-6Al-4V by Seo et al. (2005) and is found to be a good representation of the material behavior at high strain rates.The main advantages of this model are its ease of calibration and implementation and its robustness. Therefore it is very commonly used in Finite Element simulations of machining. According to Meyer and Kleponis (2001), the strain rate hardening of Ti-6Al-4V is poorly described by this model.

4.1.2 Sellars-Tegart Model

A rate dependant model for plastic flow can be written as

$$\dot{\varepsilon} = AF\sigma e^{\frac{-Q}{RT}} \tag{4.6}$$

[a] Westman (2003)
[b] Lee and Lin (1997)
[c] Meyer and Kleponis (2001)
[d] Lesuer (2000)
[e] Lesuer (2000)

$$F(\sigma) = \begin{cases} \sigma^n & if\ \alpha\sigma < 0.8 \\ e^{\beta\sigma} & if\ \alpha\sigma > 1.2 \\ (sin(\alpha\sigma))^n & for\ all\ \sigma \end{cases} \tag{4.7}$$

Lee and Lin (1997) has chosen $F(\sigma) = (sin(\alpha\sigma))^n$ and the equation 4.7 can be written as

$$\dot{\varepsilon} = A\,(sin(\alpha\sigma))^n\,\sigma e^{\frac{-Q}{RT}} \tag{4.8}$$

where Q is the activation energy, R is the gas constant and T is the absolute temperature in Kelvin. The parameters of the model are given in table 4.2.

Table 4.2: Material parameters estimated.

Reference	α	n	A
Lee and Lin (1997)	0.0012	38.01	A($\dot{\varepsilon}$)

4.1.3 Polynomial Relation Model

Westman (2003) used a polynomial model to compute the flow stress as below

$$\sigma(y) = A(T)(B + C\varepsilon^{1/n(t)}) \tag{4.9}$$
$$A(T) = a_0 + a_1T + a_2T^2 + a_3T^3 \tag{4.10}$$
$$n(T) = n_0 + n_1T \tag{4.11}$$

Where, $B, C, a_0, a_1, a_2, a_3, n_0, n_1$ are material parameters which were not published.

4.2 Physically Based Models

The physically based models used in literature can be divided into explict physical models and implicit physical models. Explicit physical models contain physical parameters computed from evolution equations and are coupled to the constitutive model. In the implicit model, the form of the constitutive equation is determined based on knowledge about the physical process. Though this approach is phenomenological, it has a strong hold on the underlying physics observed during experiments.. This approach is referred to as "model-based-phenomenology" (Frost and Ashby, 1982).

4.2.1 Meyers Model

The flow stress of Ti has been modelled by Meyers et al. (2002) as

$$\sigma = \sigma_G + C_1 \left(\frac{\dot{\epsilon}_0}{\dot{\epsilon}}\right)^{-C_3 T} + \frac{C_2}{e^{-C_4 T}}\varepsilon^n + \frac{k_s}{\sqrt{d}} \tag{4.12}$$

where σ_G is the athermal component of stress, n is the work hardening, d is the grain size and k_s is the slip term in the Hall-Petch relation. $e^{-c_4 T}$ term will reduce work hardening with the increase of temperature. C_1, C_2, C_3, C_4, k_s are material parameters which were not published.

4.2.2 Majorell Model

The total stress $\tau = \tau^* + \tau_\mu$ where τ^* is the thermally activated component of stress and τ_μ is the athermal component of stress. The thermally activated component of stress for each phase can be written as

$$\begin{aligned} \tau^*_\alpha &= \tau^0(C_{O_{eq}}) \left[1 - \left(\frac{kT}{\Delta G_{O_{eq}}} \ln \frac{\dot{\gamma}_0}{\dot{\gamma}}\right)^{\frac{1}{q_{O_{eq}}}}\right]^{\frac{1}{p_{O_{eq}}}} \\ &\quad + \tau^0(C_{Al}) \left[1 - \left(\frac{kT}{\Delta G_{Al}} \ln \frac{\dot{\gamma}_0}{\dot{\gamma}}\right)^{\frac{1}{q_{Al}}}\right]^{\frac{1}{p_{Al}}} \end{aligned} \tag{4.13}$$

$$\tau^*_\beta = \tau^0_\beta \left[1 - \left(\frac{kT}{\Delta G_\beta} \ln \frac{\dot{\gamma}_{0\beta}}{\dot{\gamma}}\right)\right]^{\frac{1}{p_\beta}} \tag{4.14}$$

The parameters of the model are given in table 4.3.

Table 4.3: Material parameters estimated by Picu and Majorell (2002).

$\tau^0(C_{O_{eq}})$	$\tau^0(C_{Al})$	τ^0_β	$G_{O_{eq}}$	G_β	$\dot{\gamma}_0$	$p_{O_{eq}}$	$q_{O_{eq}}$	p_{Al}	q_{Al}	p_β
1050	1080	1200	150	200	10^7	0.45	1.7	0.7	2.7	0.4

$$\Delta G_{Al} = \begin{cases} 400 & \text{if } T < 800\text{K} \\ 400 - 350\frac{2}{\pi}\tan^{-1}\left(\frac{T-800}{130}\right) & \text{if } T > 800\text{K} \end{cases} \tag{4.15}$$

The athermal component can be written as,

$$\tau_\mu = \zeta\mu(T)b\sqrt{\rho} + \frac{k}{\sqrt{d}} \tag{4.16}$$

where ζ and k are material parameters, $\mu(T) = 49.02 - \frac{5.821}{e^{181/T} - 1}$ is the temperature dependant shear modulus, b is the burgers vector and d is the grain size. The evolution of dislocation density is computed as

$$\frac{d\rho}{d\gamma} = \frac{d\rho}{d\gamma}|_{pr} + \frac{d\rho}{d\gamma}|_{re} \tag{4.17}$$

$$\frac{d\rho}{d\gamma}|_{pr} = a_1\sqrt{\rho} \tag{4.18}$$

$$\frac{d\rho}{d\gamma}|_{re} = -a_2\frac{\dot{\gamma}_0^{ath}}{\dot{\gamma}}\rho\left(1 - e^{-0.7R_c^4\rho^2}\right)e^{-Q/kT} \tag{4.19}$$

where $\frac{d\rho}{d\gamma}|_{pr}$ is the storage term and $\frac{d\rho}{d\gamma}|_{re}$ is the recovery term. $\dot{\gamma}_0^{ath}$ and $\dot{\gamma}$ are the reference and applied strain rate, Q is the activation energy of cross slip and recombination, R_c is the cut off radius for dislocations to climb or annihiliate and a_2 is a proportionality constant.

Total stress in alpha and beta phases is given by

$$\tau = (1 - C_\beta(T))^{0.8}\left(\tau_\alpha^* + \tau_{\mu\alpha}\right) + C_\beta(T)^{0.8}\tau_\beta^* \tag{4.20}$$

where $C_\beta(T) = \left(\frac{T}{1270}\right)^{10}$ is the temperature dependent fraction of β phase.

4.2.3 Armstrong Zerilli Model

The yield strength can be written according to Zerilli and Armstrong (1998) as

$$Y = C_0 + C_1 e^{(-C_3T + C_4\ln\dot{\varepsilon})} + C_5\varepsilon^n \tag{4.21}$$

where T is the absolute temperature, ε is the equivalent plastic strain, $\dot{\varepsilon}$ is the equivalent plastic strain rate and C_0, C_1, C_3, C_4 are material parameters to be estimated. C_5 and n are the same as B and n in the Johnson-Cook model. The parameters of the model are given in table 4.4. This model is not recommended for temperatures

Table 4.4: Parameters Estimated by Meyer and Kleponis (2001)

C_1	C_2	C_3	C_4	C_5	n
740	240	0.0024	0.00043	656	0.5

above one half of the melting point. Meyer and Kleponis (2001) reported that this model gave better predictions as compared to the Johnson-Cook model

4.2.4 Nemat-Nasser Model

The flow strength is written as

$$\begin{aligned} \tau\left(\dot{\gamma},\gamma,T\right) &= \tau^0\left\{1-\left[\frac{kT}{G_0}\left(\ln\frac{\dot{\gamma}f(\gamma,T)}{\dot{\gamma}_0}\right)\right]^{1/q}\right\}^{1/p} \\ &+ \tau_a^0\gamma^n + f(\gamma,T) \qquad (4.22) \\ f(\gamma,T) &= 1+a_0\left[1-\left(\frac{T}{T_m}\right)^2\right]\gamma^{1/2} \qquad (4.23) \end{aligned}$$

where γ and $\dot{\gamma}$ is the effective plastic strain and strain rate, T and T_m are the absolute and melting temperature respectively, τ^0 is the empirically determined effective stress, G_0 is the magnitude of energy barrier of dislocations, $\dot{\gamma}_0$ is the reference strain rate, $\tau_a^0\gamma^n$ is the athermal part of the flow stress and a_0 depends on average initial dislocation spacing. This model was fit to Ti-6Al-4V with different microstructures produced with different manufacturing techniques. The material parameters of the model are given in the table 4.5.

Table 4.5: Material Parameters Estimated by Nemat-Nasser et al. (2001)

Material	p	q	k/G_0 $_{10^{-5}\mathrm{K}^{-1}}$	$\dot{\gamma}_0$ $_{10^{10}\mathrm{s}^{-1}}$	a_0	τ^0	τ_a^0	n
Commercial[a]	1	2	6.2	1.32	2.4	1560	685	0.05
RS-HIP[b]	1	2	6.2	1.32	2.4	1620	680	0.04
RS-MIL-HIP[c]	1	2	6.2	1.32	2.4	1900	710	0.03

[a] Commercial purity Ti-6Al-4V
[b] Hot Isostatic Pressed Ti-6Al-4V
[c] Hot Isostatic Pressed material made with milled powder Ti-6Al-4V

Chapter 5

Dislocation Density Based Model

The plastic behavior of Ti-6Al-4V is complicated as it involves varying phases, textures and morphologies as explained in chapter 3. A constitutive model which should account for these phenomena should be based on the physics of material behavior.

5.1 Formulation of the model

The flow stress model is formulated on a homogeneous representative volume element and it provides a bridge between various sub-micro scale phenomena and macro scale continuum mechanics. Properties of dislocations are related to macroscopic plasticity. Plastic strain is associated to motion of dislocations, while hardening or softening is associated to interaction of dislocations. With the increase of dislocation density, the dislocations themselves get entangled and prevent further motion which results in isotropic hardening. Due to the lattice distortion around the dislocations, elastic energy is stored in the material which also hinders the movement of the dislocations contributing to isotropic hardening. However, the internal stresses can also support dislocation movement in the opposite direction resulting in the so called "Bauschinger effect" or kinematic hardening. Recovery and recrystallization are two competing restoration mechanisms and they balance the strain hardening. In order to compute evolution of the material state, dislocation density and vacancy concentration are used as internal state variables in this model.

5.2 Bridging Scales

The proposed model has capability to connect to the microstructure of the material. This model is formulated on a homogeneous representative volume element and it provides a bridge between sub-micro scale phenomena and macro scale continuum mechanics (see figure 5.1). The flow of data from different scales are shown in figure 5.2.

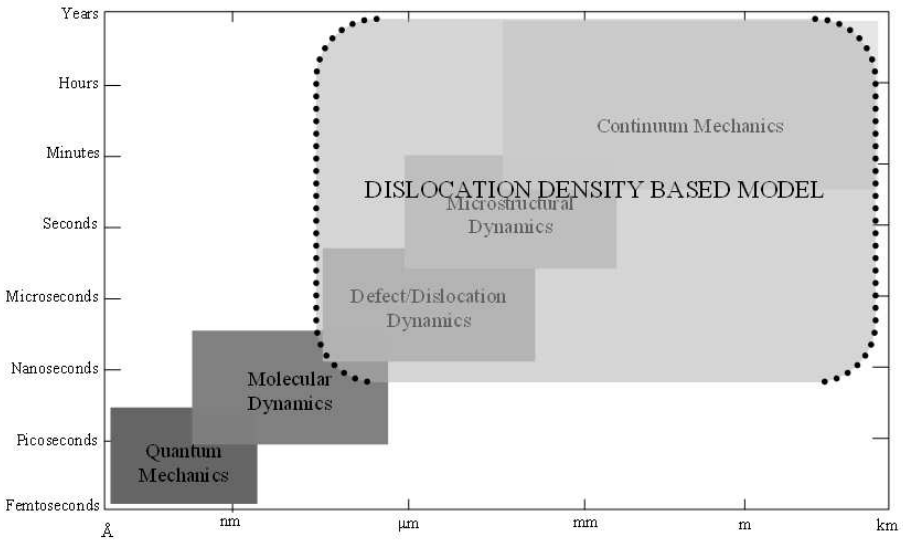

Figure 5.1: Length and time scales of deformation.

5.2.1 Flow Stress

The flow stress is assumed to consist of two parts (Bergström, 1969, Kocks, 1976, Seeger, 1956),

$$\sigma_y = \sigma_G + \sigma^* \tag{5.1}$$

where, σ_G is the athermal stress contribution from the long-range interactions of the dislocation substructure. The second term σ^*, is the friction stress needed to move dislocations through the lattice and to pass short-range obstacles. Thermal vibrations can assist dislocations to overcome these obstacles. This formulation is very much in accordance to the material behavior demonstrated by Conrad (1981) in equation (3.1).

Long range flow stress contribution

In an isotropic and homogeneous lattice, stress field surrounding a screw dislocation can be written as

$$\tau = \frac{Gb}{2\pi r} \tag{5.2}$$

where, G is the shear modulus, b is the Burgers vector and r is the radius of the Burgers circuit.

If we assume that the number of dislocations intersecting a unit area is ρ, then the mean distance between dislocations is $\sqrt{\rho}^{-1}$. Drawing from this relation, the long-range term of equation (5.1) is derived by Seeger (1956) as,

$$\sigma_G = m\alpha Gb\sqrt{\rho_i} \tag{5.3}$$

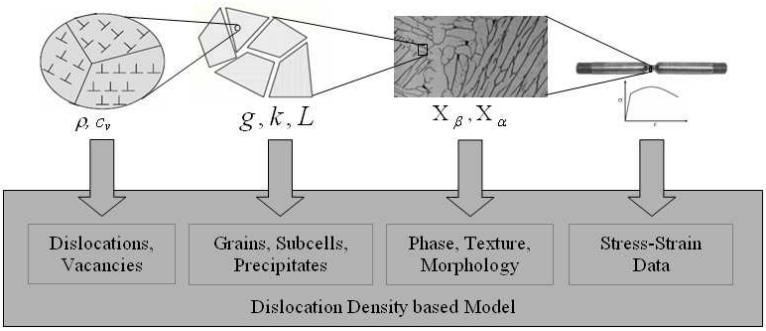

Figure 5.2: Data Flow in dislocation density based model.

where m is the Taylor orientation factor translating the effect of the resolved shear stress in different slip systems into effective stress and strain quantities. Furthermore, α is a proportionality factor and ρ_i is the immobile dislocation density. The shear modulus can be computed from the Youngs modulus (E) and Poisson ratio (ν) as,

$$G = \frac{E}{2(1+\nu)} \tag{5.4}$$

Short range flow stress contribution

The strength of obstacles, which a dislocation encounters during motion determines the dependence of flow strength on applied strain rate. The dislocation velocity is related to plastic strain rate via the Orowan equation (Orowan, 1948)

$$\dot{\varepsilon}^p = \frac{\rho_m b \bar{\nu}}{m} \tag{5.5}$$

where $\bar{\nu}$ is the average velocity of mobile dislocations (ρ_m). This velocity is related to the time taken by a dislocation to pass an obstacle most of which is the waiting time. The velocity is written according to Frost and Ashby (1982) as,

$$\bar{\nu} = \Lambda \nu_a e^{-\Delta G/kT} \tag{5.6}$$

where Λ is the mean free path, ν_a is the attempt frequency, ΔG is the activation energy, k is the Boltzmann constant and T is the temperature in Kelvin. Here, $e^{-\Delta G/kT}$ can be considered as the probability that the activation energy is availabe.

$$\dot{\bar{\varepsilon}}^p = f e^{-\Delta G/kT} \tag{5.7}$$

The form of the function f and ΔG depend on the applied stress, strength of obstacles etc. The stress available to move a dislocation past an obstacle is the difference between applied stress and the long-range flow stress component. Since the effective stress in the plasticity model is equal to the flow stress, $f = f(\bar{\sigma} - \sigma_G) = f(\sigma^*)$.

If obstacles of strength K as shown in figure 5.3 are arranged in a lattice with mean spacing l, under the influence of a resolved shear stress τ, the net applied forward force is $\tau b l$. If the dislocation moves from x_1 to x_2 the net energy required is the area

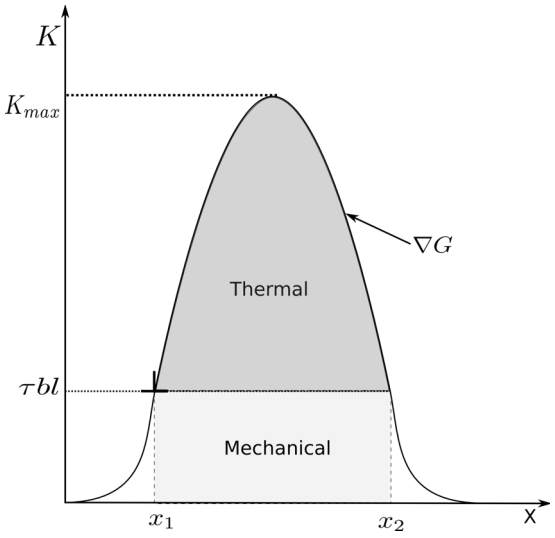

Figure 5.3: Obstacle Resistance

under the curve and part of it is supplied as the mechanical work $\tau bl(x_2 - x_1)$. The remaining energy ΔG is the free energy of activation which can be written according to Kocks et al. (1975) as

$$\Delta G = \Delta F \left[1 - \left(\frac{\sigma^*}{\sigma_{ath}}\right)^p\right]^q \tag{5.8}$$
$$0 \leq p \leq 1$$
$$1 \leq q \leq 2$$

Here, $\Delta F = \Delta f_0 G b^3$ is the activation energy necessary to overcome lattice resistance in the absence of any external force and $\sigma_{ath} = \tau_0 G$ is the shear strength in the absence of thermal energy. The parameters p and q determine the shape of the barrier either sinusoidal or hyperbolic or somewhere in between. Some guidelines for selection of Δf_0 and τ_0 are given in Table 5.1. Here l is the mean spacing of the obstacles; either precipitates or solutes. The strain rate dependent part of the yield stress from equation (5.1) can be derived according to the Kocks-Mecking formulation (Kocks et al., 1975, Mecking and Kocks, 1981) as

$$\sigma^* = \tau_0 G \left[1 - \left[\frac{kT}{\Delta f_0 G b^3} \ln\left(\frac{\dot{\varepsilon}^{ref}}{\dot{\varepsilon}^p}\right)\right]^{1/q}\right]^{1/p} \tag{5.9}$$

Here $\dot{\varepsilon}^{ref}$ is the reference strain rate.

5.2.2 Evolution of immobile dislocation density

The basic components for the yield stress in equation (5.1) are obtained from equations (5.3 and 5.9). However, the evolution of ρ_i in equation (5.3) needs to be com-

Table 5.1: Activation energy factor and shear strength of different obstacles from Frost and Ashby (1982)

Obstacle Strength	Δf_0	τ_0	Example
Strong	2	$> \frac{b}{l}$	Strong precipitates
Medium	$0.2 - 1.0$	$\approx \frac{b}{l}$	Weak precipitates
Weak	< 0.2	$\ll \frac{b}{l}$	Lattice Resistance,

puted. The model for evolution of the immobile dislocation density has two parts; hardening and restoration.

$$\dot{\rho_i} = \dot{\rho_i}^{(+)} + \dot{\rho_i}^{(-)} \tag{5.10}$$

Hardening Process

It is assumed that mobile dislocations move, on average, a distance Λ (mean free path), before they are immobilized or annihilated. According to the Orowan equation, density of mobile dislocations and their average velocity are proportional to the plastic strain rate. It is reasonable to assume that increase in immobile dislocation density also follow the same relation. This leads to

$$\dot{\rho_i}^{(+)} = \frac{m}{b}\frac{1}{\Lambda}\dot{\bar{\varepsilon}}^p \tag{5.11}$$

where m is the Taylor orientation factor. The mean free path can be computed from the grain size (g) and dislocation subcell or subgrain diameter (s) as,

$$\frac{1}{\Lambda} = \left(\frac{1}{g} + \frac{1}{s} + others\right) \tag{5.12}$$

where *others* denote contributions from obstacles like precipitates, interstitial elements, martensite lathes etc. The effect of grain size on flow stress known as Petch-Hall relation, is accounted via this term. Models for recrystallization, grain growth, precipitation, dissolution etc can be included here (Babu, 2007).

The formation and evolution of subcells has been modelled using a relation proposed by Holt (1970) with s_∞ as the minimum subcell size.

$$s = K_c\frac{1}{\sqrt{\rho_i}} + s_\infty \tag{5.13}$$

Restoration Processes

Motion of vacancies is related to recovery of dislocations. This occur usually at elevated temperatures and therefore is a thermally activated reorganization process. Creation of vacancy increases entropy but consumes energy and its concentration increases with temperature and deformation. In high stacking fault materials, recovery

process might balance the effects of strain hardening leading to a constant flow stress.

Recovery by Glide:
Kocks et al. (1975) has derived an equation for evolution of mobile dislocation density which can be written as

$$\dot{\rho}_m = \rho_m \bar{\nu} \left(\frac{1}{\Lambda_{back}} - \frac{1}{\Lambda} \right) \tag{5.14}$$

where, Λ_{back} is the distance travelled by a previously emitted dislocation and $\bar{\nu}$ is the spacial average velocity of mobile dislocations.

Based on the formulation by Bergström (1983), the immobile dislocation density is proportional to the plastic strain rate.

$$\dot{\rho_i}^{(-)} = \Omega \rho_i \dot{\bar{\varepsilon}}^p \tag{5.15}$$

where Ω is a function dependent on temperature. This is analogous to Kocks formulation as ρ_i and $\dot{\bar{\varepsilon}}^p$ are proportional to ρ_m and $\bar{\nu}$ respectively.

Recovery by Climb:
In addition to dislocations, vacancies are also created during plastic deformation (Fridel, 1964). This has significant effect on diffusion controlled processes such as climb and dynamic strain ageing. Militzer et al. (1994) proposed a model based on Sandstrom and Lagneborg (1975) and Mecking and Estrin (1980). With a modification of the diffusivity according to equation (5.26), this can be written as

$$\dot{\rho_i}^{(-)} = 2 c_\gamma D_l \frac{c_v}{c_v^{eq}} \frac{G b^3}{kT} \left(\rho_i^2 - \rho_{eq}^2 \right) \tag{5.16}$$

where, c_v^{eq} and c_v are equilibrium and current vacancy concentrations and c_γ, a material coefficient.

5.2.3 Evolution of excess vacancy concentration

The concentration of vacancies attain equilibrium if left undisturbed in isothermal conditions. When subjected to deformation or temperature change, the material generates excess vacancies. The model considered here is only concerned with monovacancies. The equilibrium concentration of vacancies at a given temperature according to Cahn and Peter (1996a), Reed-Hill and Abbaschian (1991) is

$$c_v^{eq} = e^{\frac{\Delta S_{vf}}{k}} e^{-\frac{Q_{vf}}{kT}} \tag{5.17}$$

where, ΔS_{vf} is the increase in entropy while creating a vacancy and Q_{vf} is the activation energy for vacancy formation.

Vacancy Creation and Annihilation

Militzer et al. (1994) proposed a model for excess vacancy concentration with generation and annihilation components as

$$\dot{c_v}^{ex} = \dot{c}_v - \dot{c}_v^{eq} = \left[\chi \frac{\sigma b}{Q_{vf}} + \zeta \frac{c_j}{4b^2} \right] \frac{\Omega_0}{b} \dot{\bar{\varepsilon}} - D_{vm} \left[\frac{1}{s^2} + \frac{1}{g^2} \right] (c_v - c_v^{eq}) \tag{5.18}$$

Here, $\chi = 0.1$ is the fraction of mechanical energy spent on vacancy generation, Ω_0 is the atomic volume and ζ is the neutralization effect by vacancy emitting and absorbing jogs which is computed as below.

$$\zeta = \begin{cases} 0.5 - \zeta_0 c_j & if\ c_j \leq 0.5/\zeta_0 \\ 0 & if\ c_j > 0.5/\zeta_0 \end{cases}$$
$$\zeta_0 = 10 \tag{5.19}$$

The concentration of jogs is given as

$$c_j = e^{-\frac{Q_{jf}}{kT}}; \quad Q_{jf} = \frac{Gb^3}{4\pi(1-\nu)} \tag{5.20}$$

where Q_{jf} is the activation energy of jog formation.

Assuming that only long range stress contributes to vacancy formation and introducing mean free path, equation (5.18) becomes,

$$\dot{c_v}^{ex} = \left[\chi \frac{m\alpha G b^2}{Q_{vf}} + \zeta \frac{c_j}{4b^2}\right] \frac{\Omega_0}{b} \dot{\bar{\varepsilon}} - D_{vm} \left[\frac{1}{\Lambda^2}\right] (c_v - c_v^{eq}) \tag{5.21}$$

Vacancy Creation from Temperature Change

Additionally, excess vacancy concentration can be driven by temperature change as

$$\dot{c_v}^{ex} = c_v^{eq} \left(\frac{Q_{vf}}{T^2}\right) \Delta T \tag{5.22}$$

5.2.4 Model for Self Diffusion

Diffusion occurs by the motion of defects like vacancies and interstitial atoms and by atomic exchange. But vacancy motion is the predominant diffusion mechanism due to the lower activation energy of vacancy formation (Fridel, 1964). The self diffusion coefficient can be written according to
Reed-Hill and Abbaschian (1991) as

$$D_l = a^2 \nu e^{\frac{\Delta S_{vm} + \Delta S_{vf}}{k}} e^{-\frac{Q_{vm}+Q_{vf}}{kT}} = D_{l0} e^{-\frac{Q_v}{kT}} \tag{5.23}$$

where, a is the lattice constant, ν is the lattice vibration frequency, ΔS_{vm} is the entropy increase due to the motion of a vacancy, Q_{vm} is the energy barrier to be overcome for vacancy motion and D_{l0} is the activity factor of lattice diffusion.

Vacancy migration leads to vacancy annihilation and it follows an Arrhenius type relation as below.

$$D_{vm} = a^2 \nu e^{\frac{\Delta S_{vm}}{k}} e^{-\frac{Q_{vm}}{kT}} \tag{5.24}$$

Introducing the equilibrium concentration of vacancy from equation (5.17), self diffusivity can be written as

$$D_l = c_v^{eq} D_{vm} \tag{5.25}$$

Thus the self-diffusivity is the product of vacancy diffusivity and its equilibrium concentration. This can be rewritten generically for any concentration of vacancy as

$$D_l^* = \frac{c_v}{c_v^{eq}} D_l \tag{5.26}$$

Lattice diffusivity of α and β phases differ in many orders of magnitude which results in a jump at the β-transus temperature (Mishin and Herzig, 2000). This transition is modelled by scaling the diffusivity with the volume fraction of each phases.

$$D_l = D_\alpha \cdot (1-f)^w + D_\beta \cdot f^w \tag{5.27}$$

where $f = f(T)$ is the volume fraction of β phase.

Reed-Hill and Abbaschian (1991) proposed an Arrhenius type equation for grain boundary diffusion similar to equation (5.24). The effect of grain boundary diffusion can be neglected in the proposed model because of the large grain size of the material considered. Since the basic mechanisms of grain boundary and dislocation core (pipe) diffusion are the same (Shewmon, 1963), a similar formulation is employed here for pipe diffusion.

$$D_p = D_{p0} e^{-\frac{Q_p}{kT}} \tag{5.28}$$

where, D_{p0} is the frequency factor and Q_p is the activation energy.

The total diffusive flux in the material is enhanced by the short circuit diffusion which is dependant on the relative cross sectional area of pipe and matrix. According to the model proposed by Militzer et al. (1994), Porter and Easterling (1992), the apparent diffusivity can be written as

$$D_{app} = D_l + N D_p \tag{5.29}$$

where, N is the cross sectional area of pipes per unit area of matrix.

$$N = \frac{n_a^p n_\rho}{N_a^l} \tag{5.30}$$

where, n_a^p is the number of atoms that can fill the cross-sectional area of a dislocation, n_ρ is the number of dislocations intersecting a unit area and N_a^l is the number of atoms per unit area of lattice.

5.2.5 Stress-Update

To compute the flow stress evolution for arbitrary paths, a radial return algorithm can be used (Simo and Taylor, 1986, Simo and Hughes, 1998). This requires hardening modulus and updated internal variables for each time increment. In the proposed model, $\sigma_y = \sigma_y(\bar{\varepsilon}^p, \rho_i, c_v)$ where ρ_i and c_v are described by a coupled set of differential equations. These internal variables can be written in vector form as $\mathbf{q}^T = [q_1, q_2] = [\rho_i, c_v]$. An implicit iterative procedure is used in every time increment to calculate its evolution as given below.

$$\mathbf{H}^T = [H_1, H_2] = 0 \tag{5.31}$$

$$H_1 = \Delta q_1 - \left[\frac{m}{b\Lambda}\Delta\bar{\varepsilon}^p - \Omega q_1 \Delta\bar{\varepsilon}^p - 2c_\gamma D_l q_2 \frac{Gb^3}{kT}\left(q_1^2 - \rho_{eq}^2\right)\rho_{i0}\Delta t\right] \tag{5.32}$$

$$H_2 = \Delta q_2 - \left[\chi\frac{\Omega_0 m\alpha Gb}{Q_{vf}}\sqrt{q_1}\Delta\bar{\varepsilon}^p + \zeta\frac{c_j\Omega_0}{4b^3}\Delta\bar{\varepsilon}^p - \frac{D_{vm}}{\Lambda^2}\left(q_2 - c_v^{eq}\right)\Delta t + c_v^{eq}\left(\frac{Q_{vf}}{T^2}\right)\Delta T\right] \tag{5.33}$$

The iterative change in $\mathbf{q}$ can be written as

$$d\mathbf{q} = -\left[\frac{\partial \mathbf{H}_{(i)}}{\partial \mathbf{q}}\right]^{-1} \mathbf{H}_{(i)} \tag{5.34}$$

where, i is the iteration counter. The value of the state variables can be updated as

$$\mathbf{q}_{(i+1)} = \mathbf{q}_{(i)} + d\mathbf{q} \tag{5.35}$$

The iterative solution procedure for the internal state variables in equation (5.34) involve the computation of the following derivatives.

$$\begin{aligned}
\frac{\partial H_1}{\partial q_1} &= 1 + \Omega q_1 \Delta\bar{\varepsilon}^p + 4c_\gamma D_l \frac{q_2}{c_v^{eq}} \frac{Gb^3}{kT} q_1 \Delta t && (5.36)\\
\frac{\partial H_1}{\partial q_2} &= -2c_\gamma D_l \frac{1}{c_v^{eq}} \frac{Gb^3}{kT} \left(q_1^2 - \rho_{eq}^2\right) \Delta t && (5.37)\\
\frac{\partial H_2}{\partial q_1} &= -0.5\chi \frac{\Omega_0 m \alpha G b}{Q_{vf}\sqrt{q_1}} \Delta\bar{\varepsilon}^p && (5.38)\\
\frac{\partial H_2}{\partial q_2} &= 1 + \frac{D_{vm}}{\Lambda^2} \Delta t && (5.39)
\end{aligned}$$

The hardening modulus is defined as

$$\begin{aligned}
H' &= \frac{d\sigma_y(\mathbf{q})}{d\bar{\varepsilon}^p} = \frac{\partial \sigma_y}{\partial \mathbf{q}} \frac{\partial \mathbf{q}}{\partial \bar{\varepsilon}^p} \\
&= \frac{\partial \sigma_G}{\partial \rho_i} \left[\frac{\partial \rho_i}{\partial \bar{\varepsilon}^p} + \frac{\partial \rho_i}{\partial c_v} \frac{\partial c_v}{\partial \bar{\varepsilon}^p}\right] + \frac{\partial \sigma^*}{\partial \bar{\varepsilon}^p} && (5.40)
\end{aligned}$$

Equation (5.40) requires evaluation of the following derivatives.

$$\begin{aligned}
\frac{\partial \sigma_G}{\partial \rho_i} &= \frac{m\alpha G b}{2\sqrt{q_1}} && (5.41)\\
\frac{\partial \rho_i}{\partial \bar{\varepsilon}^p} &= \frac{m}{b\Lambda} - \Omega q_1 && (5.42)\\
\frac{\partial \rho_i}{\partial c_v} &= -2c_\gamma D_l \frac{1}{c_v^{eq}} \frac{Gb^3}{kT} \left(q_1^2 - \rho_{eq}^2\right) \Delta t && (5.43)\\
\frac{\partial c_v}{\partial \bar{\varepsilon}^p} &= \chi \frac{\Omega_0 m \alpha G b}{Q_{vf}} \sqrt{q_1} + \zeta \frac{c_j \Omega_0}{4b^3} && (5.44)\\
\frac{\partial \sigma^*}{\partial \bar{\varepsilon}^p} &= \frac{\sigma_{th} \left(\frac{kTlog\left(\frac{\dot{\varepsilon}^{ref}}{\dot{\bar{\varepsilon}}^p}\right)}{\Delta f_0 G b^3}\right)^{\frac{1}{q}}}{pq\dot{\bar{\varepsilon}}^p log\left(\frac{\dot{\varepsilon}^{ref}}{\dot{\bar{\varepsilon}}^p}\right)\Delta t} \left(1 - \left(\frac{kTlog\left(\frac{\dot{\varepsilon}^{ref}}{\dot{\bar{\varepsilon}}^p}\right)}{\Delta f_0 G b^3}\right)^{\frac{1}{q}}\right)^{\frac{1}{p}-1} && (5.45)
\end{aligned}$$

5.3 Optimization of the model

The parameters for the model are obtained using an in-house Matlab® based toolbox. This toolbox uses Matlab®'s constrained minimization routine and can handle multiple experiments for optimization (Domkin and Lindgren, 2003). The shear modulus is computed according to equation (5.4) using the temperature dependant Youngs modulus given in figure 3.7 and a constant Poissons ratio of 0.3. The thermal component of strain is given in figure 3.7.

According to Hernan et al. (2005), the entropy of vacancy migration for HCP metals lies in the range $(0.9 - 1.6)k$. Here ΔS_{vm} is assumed to be equal to k. The activation energy of vacancy formation (Q_{vf}), measured by Novikov et al. (1980) for elemental Ti is used in this work. Conrad (1981) measured the dislocation density of undeformed Ti alloy with (0.1 - 1.0) at% O_{eq} to be of the order of $10^{13}m^{-2}$. This should apply for Ti-6Al-4V also. Figure 5.4 shows the apparent diffusivity of Ti-

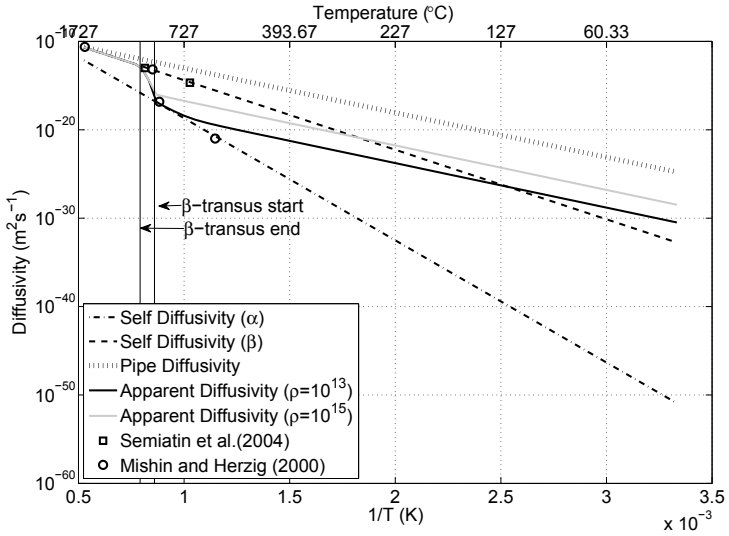

Figure 5.4: Self diffusion

6Al-4V for different values of dislocation density which correspond to annealed and deformed material. Enhanced diffusivity due to pipe diffusion has a significant effect at low temperature ($< 0.5T_{melt}$). At high temperature, it is the lattice diffusivity which has significance. The activity factor of pipe diffusion (D_{p0}) is assumed to be of the same order as that of lattice diffusion.

The different parameters of the model obtained after fitting to experiments are shown in the figure 5.5. The parameters p and q of the short range term in equation 5.9 jump in magnitude between 800 and 900 °C. This can be attributed to the onset of β-transition. The temperature independant parameters of the model and other physical data of the material are given in table 5.3

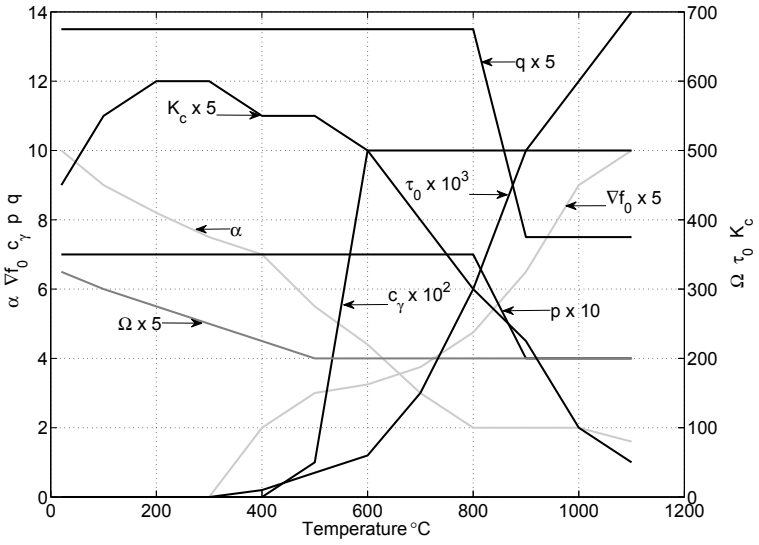

Figure 5.5: Temperature dependant parameters for the model

Parameter	Dimension	Value	Reference
T_{melt}	°C	1600	
$T_{\beta-transus}$	°C	890	
k	JK^{-1}	$1.38 \cdot 10^{-23}$	
b	m	$2.95 \cdot 10^{-10}$	a
ΔS_{vm}	JK^{-1}	$1.38 \cdot 10^{-23}$	f
$D_{\alpha 0}$	$m^2 s^{-1}$	$5.0 \cdot 10^{-6}$	d
$D_{\beta 0}$	$m^2 s^{-1}$	$3.0 \cdot 10^{-7}$	d
D_{p0}	$m^2 s^{-1}$	10^{-8}	f
Q_{vf}	J	$1.9 \cdot 10^{-19}$	b
Q_{vm}	J	$2.49 \cdot 10^{-19}$	a
Q_{β}	J	$2.5 \cdot 10^{-19}$	d
Q_p	J	$1.61 \cdot 10^{-19}$	a
n_a^p	-	2	e
n_{ρ}	-	ρ_i	e
N_a^l	-	10^{19}	f
Ω_0	m^3	$1.76 \cdot 10^{-29}$	a
g	m	$20.0 \cdot 10^{-6}$	e
s_{∞}	m	$6.0 \cdot 10^{-7}$	g
$\dot{\varepsilon}_{ref}$	s^{-1}	10^6	a
ρ_{i0}	m^{-2}	10^{13}	c
ρ_{eq}	m^{-2}	10^{10}	g

[a]Frost and Ashby (1982)
[b]Novikov et al. (1980)
[c]Conrad (1981)
[d]Mishin and Herzig (2000)
[e]Calculated or Measured Value
[f]Assumed Value
[g]Optimization Parameter

Table 5.2: Constant parameters for the model

5.4 Model and experiments

Comparison of experiments and predictions of the model using the previously given parameters are plotted in the figures 5.6 to 5.9. The dots denote measurements and lines denote calculations. Compression tests performed at the nominal temperatures (20, 100, 200, 300, 400, 500, 600, 700, 800, 900, 1000 and 1100) °C have been used to calibrate the model. The actual temperature recorded from the thermocouple deviated slightly from the nominal values and was accounted for in the computation. The compression tests performed at 20 °C to 500 °C resulted in hardening followed by fracture and at temperatures between 600 °C to 900 °C resulted in flow softening after the initial hardening. The deformation mechanisms leading to flow softening is not well understood. Park et al. (2008) has reported that grain boundary sliding (GBS) controlled by grain boundary diffusion is the dominant mechanism responsible for this behavior. Ti-6Al-4V undergoes dynamic recrystallization (DRx) at elevated temperatures (Abe et al., 2003). DRx can lead to flow softening because the new grains have lower dislocation density than the existing ones. The tests from 1000 °C to 1100 °C showed elastic-perfectly-plastic behavior. Between 20 to 500 °C, the flow stress is less sensitive to strain rate.

Comparison of stress relaxation measurements done by Donachie (1988) and the model predictions are given in figure 5.9. Though, the exact boundary conditions of the experiments and the composition of the alloy are not known, this comparison demonstrates the capacity of the model to compute the decay of stress with time. The model underestimates initial relaxation of stress. This maybe ascribed to mechanisms of GBS or DRx responsible for flow softening which is not included in this work.

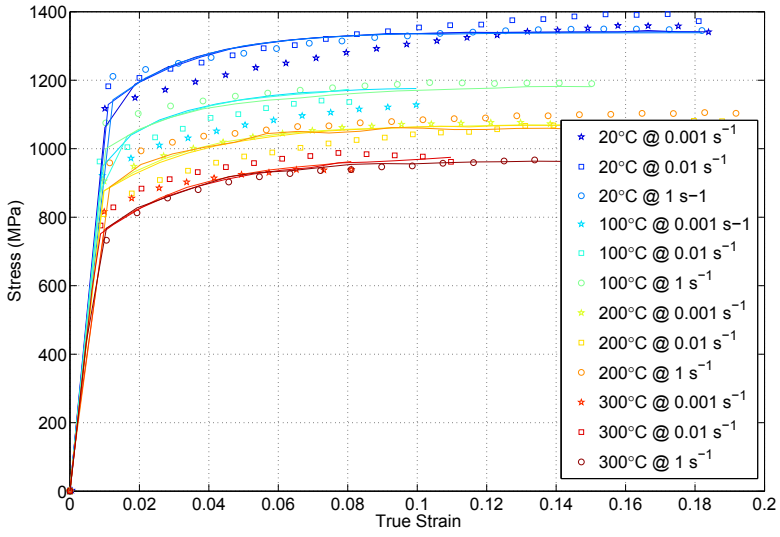

Figure 5.6: Measured and computed stress-strain curve for 20 °C to 300 °C.

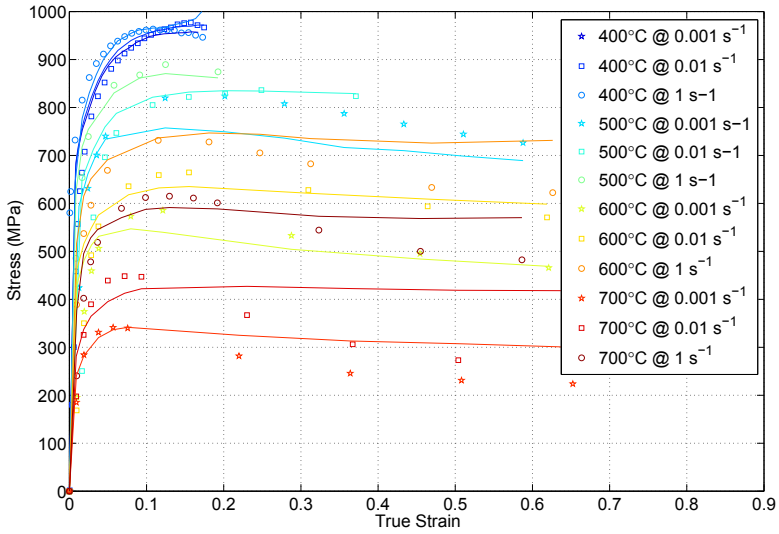

Figure 5.7: Measured and computed stress-strain curve for 400 °C to 700 °C.

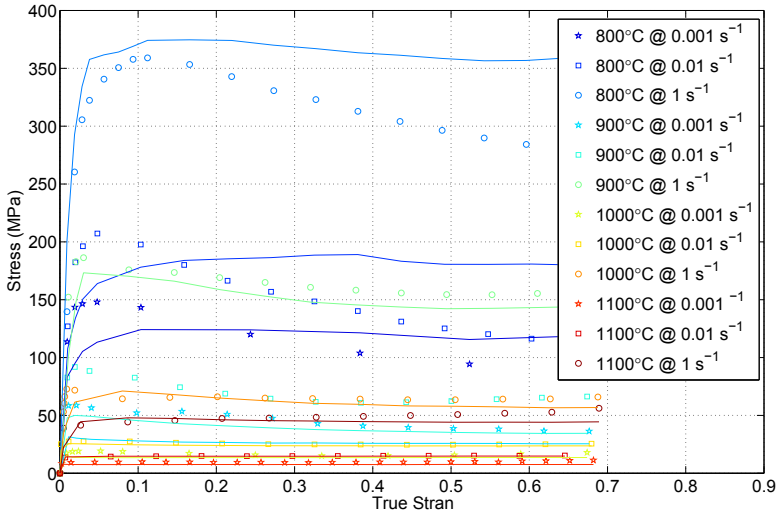

Figure 5.8: Measured and computed stress-strain curve for 800 °C to 1100 °C.

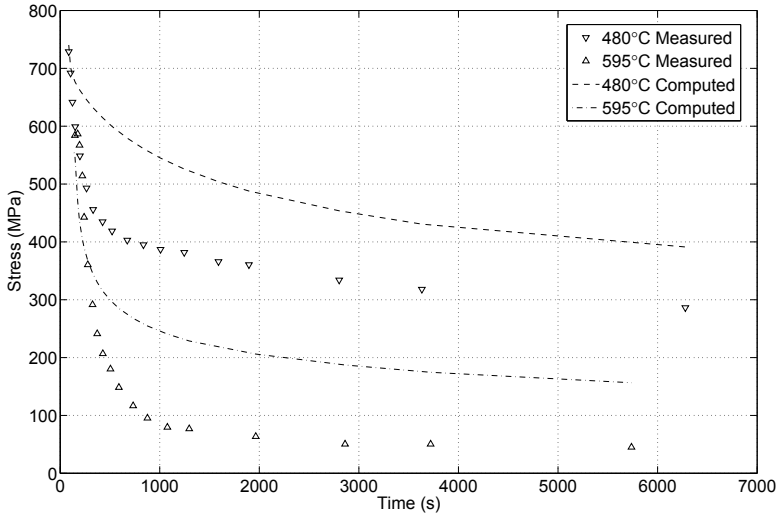

Figure 5.9: Measured and computed stress relaxation at 480 °C and 595 °C.

Chapter 6

Conclusions and Future Work

A constitutive model based on the physics of the material behavior is developed. The model can give predictions with adequate accuracy for simulations of various manufacturing processes like forming, welding, metal deposition and heat treatment. Some of the parameters used in the model are available from measurements outside the domain of classical mechanical testing. Since some of these parameters are not available for this specific alloy, the data for elemental Ti has been used here. This model is formulated using a rate dependant yield surface framework which can be implemented in most commerical finite element packages. Therefore the logic for stress update described here is directly applicable for large scale simulations.

Some additional measurements are necessary to validate the various submodels employed here *viz*; the substructure evolution. Also, the current plasticity model has to be extended with submodels for globularisation, recrystallisation, and localisation. EBSD is a very useful technique to study the structure of the material at different scales. In-situ measurements of DRy and DRx using EBSD coupled with the numerical simulations have proven to be a valuable tool towards gaining a better understanding of the structure property relationships (Piazolo et al., 2004). Since the proposed flow stress model follow a clear physical framework, new submodels can be added with relative ease.

Bibliography

H. Abe, T. Furuhara, and T. Maki. Dynamic recrystallization of Ti-6Al-4V alloy. *Current Advances in Materials and Processes*, 16(6):1479, 2003.

Bijish Babu. Dislocation density based constitutive model for Ti-6Al-4V : including recovery and recrystallisation. In Eugenio Onate, Roger Owen, and Benjamin Suarez, editors, *Computational plasticity : Fundamentals and Applications*, volume 2, pages 631–634, 2007. ISBN 978-84-96736-29-0.

M. J. R. Barboza, E. A. C. Perez, M. M. Medeiros, D. A. P. Reis, M. C. A. Nono, F. Piorino Neto, and C. R. M. Silva. Creep behavior of Ti-6Al-4V and a comparison with titanium matrix composites. *Materials Science and Engineering: A*, 428(1-2): 319, 2006.

M. R. Barnett, G. L. Kelly, and P. D. Hodgson. Predicting the critical strain for dynamic recrystallization using the kinetics of static recrystallization. *Scripta Materialia*, 43(4):365, 2000.

Y. Bergström. Dislocation model for the stress-strain behaviour of polycrystalline alpha-iron with special emphasis on the variation of the densities of mobile and immobile dislocations. *Materials Science & Engineering*, 5:193–200, 1969.

Y. Bergström. The plastic deformation of metals – a dislocation model and its applicability. *Reviews on Powder Metallurgy and Physical Ceramics*, (2/3):79–265., 1983.

S. Bruschi, S. Poggio, F. Quadrini, and M. E. Tata. Workability of Ti-6Al-4V alloy at high temperatures and strain rates. *Materials Letters*, 58(27-28):3622, 2004.

Robert W. Cahn and Haasen Peter. *Physical Metallurgy*, volume 1. North-Holland Publishers, Amsterdam, NL:, 4 edition, 1996a.

Robert W. Cahn and Haasen Peter. *Physical Metallurgy*, volume 3. North-Holland Publishers, Amsterdam, NL:, 4 edition, 1996b.

D. R. Chichili, K. T. Ramesh, and K. J. Hemker. The high-strain-rate response of alpha-titanium: Experiments, deformation mechanisms and modeling. *Acta Materialia*, 46(3):1025, 1998.

Hans Conrad. Effect of interstitial solutes on the strength and ductility of titanium. 26(2-4):123, 1981.

R. Ding and Z. X. Guo. Microstructural evolution of a Ti-6Al-4V alloy during [beta]-phase processing: experimental and simulative investigations. *Multiscale Materials Modelling*, 365(1-2):172, 2004.

R. Ding, Z. X. Guo, and A. Wilson. Microstructural evolution of a Ti-6Al-4V alloy during thermomechanical processing. *Materials Science and Engineering A*, 327 (2):233, 2002.

Konstantin Domkin. *Constitutive models based on dislocation density: formulation and implementation into finite element codes*. PhD thesis, Luleå Technical Univeristy, 2005. Dislocation Density.

Konstantin Domkin and Lars-Erik Lindgren. Dislocation density based models of plastic hardening and parameter identification. In *The 7th International Conference on Computer Plasticity*, COMPLAS, April 2003.

Jr. Matthew J. Donachie. *Titanium - A Technical Guide*. ASM International, 1988.

J Fridel. *Dislocations*, volume 3 of *International Series of Monographs on Solid State Physics*. Pergamon Press, 1964.

H. J. Frost and M. F. Ashby. *Deformation-Mechanism Maps: The Plasticity and Creep of Metals and Ceramics*. Paperback, 1982.

H. Fujii and H. G. Suzuki. A model for ductility loss at intermediate temperatures in an alpha+beta titanium alloy. *Scripta Metallurgica et Materialia*, 24(10):1843–1846, 1990.

G. Gottstein. *Physical Foundations of Material Science*. Springer-Verlag, 2004. ISBN 3-540-40139-3.

Ruiz Diego Hernan, Gribaudo Luis Maria, and Monti Ana Maria. Self-diffusion in the hexagonal structure of zirconium and hafnium: computer simulation studies. *Materials Research*, 8:431–434, 12 2005. ISSN 1516-1439.

Richard W. Hertzberg. *Deformation and Fracture Mechanics of Engineering Materials*. Wiley, 4 edition, 1995.

D. L. Holt. Dislocation cell formation in metals. *Journal of applied physics*, 41(8): 3197, 1970. 0021-8979.

Derek Hull and D. J. Bacon. *Introduction to Dislocations*. Butterworth-Heinemann, 2001. ISBN 0750646810.

F. J. Humphreys and M Hatherly. *Recrystallization and Related Annealing Phenomena*. Elsivier, Kidlington, Oxford, 2 edition, 2004.

C. Williams James and Gerd Lutjering. *Titanium*. Springer - Verlag, 2003.

K. Janghorban and S. Esmaeili. Deformation-mechanism map for Ti-6Al alloy. *Journal of Materials Science*, V26(12):3362, 1991. 10.1007/BF01124686.

A. J. Wagoner Johnson, C. W. Bull, K. S. Kumar, and C. L. Briant. The influence of microstructure and strain rate on the compressive deformation behavior of Ti-6Al-4V. *Metallurgical and Materials Transactions*, 34A(2):295–306, 2003a. 10735623.

A. J. Wagoner Johnson, K. S. Kumar, and C. L. Briant. Deformation mechanisms in Ti-6Al-4V/Tic composites. *Metallurgical and Materials Transactions*, 34A(9): 1869–1877, 2003b. 10735623.

C. H. Johnson, S. K. Richter, C. H. Hamilton, and J. J. Hoyt. Static grain growth in a microduplex Ti-6Al-4V alloy. *Acta Materialia*, 47(1):23–29, 1998.

Gordon R. Johnson and William H. Cook. Fracture characteristics of three metals subjected to various strains, strain rates, temperatures and pressures. *Engineering Fracture Mechanics*, 21(1):31–48, 1985.

S V Kailas, Y. V. R. K. Prasad, and S. K. Biswas. Flow instabilities and fracture in Ti-6Al-4V deformed in compression at 298-673K. *Metallurgical and Materials Transactions A*, 25A(10):2173–2179, 1994. Pdf of this document is not availabe.

Akhtar S. Khan, Rehan Kazmi, Babak Farrokh, and Marc Zupan. Effect of oxygen content and microstructure on the thermo-mechanical response of three Ti-6Al-4V alloys: Experiments and modeling over a wide range of strain-rates and temperatures. *nternational Journal of Plasticity*, 23(7):1105–1125, 2007.

T. Knudsen, W. Q. Cao, A. Godfrey, Q. Liu, and Niels Hansen. Stored energy in nickel cold rolled to large strains, measured by calorimetry and evaluated from the microstructure. *Metallurgical and Materials Transactions A*, 39(2):430–440, 2008. 10.1007/s11661-007-9421-1.

U. F. Kocks, A. S. Argon, and M. F. Ashby. *Thermodynamics and Kinetics of Slip*, volume 19 of *Progress in Material Science*. Pergamon Press, 1975.

U.F. Kocks. Laws for work-hardening and low-temperature creep. *Journal of Engineering Materials and Technology, Transactions of the ASME*, 98 Ser H(1):76–85, 1976.

Woei-Shyan Lee and Ming-Tong Lin. The effects of strain rate and temperature on the compressive deformation behaviour of Ti-6Al-4V alloy. 71(2):235, 1997.

Donald R. Lesuer. Experimental investigations of material models for Ti-6Al-4V titanium and 2024-T3 aluminum, 2000.

L X; Peng D S Li. Development of constitute equations for Ti-6Al-4V alloy under hot-working condition. *Acta Metallurgica Sinica (English Letters)*, 13(1):263–269, 2000.

Lars-Erik Lindgren, Konstantin Domkin, and Hansson Sofia. Dislocations, vacancies and solute diffusion in physical based plasticity model for AISI 316La. *Mechanics of Materials*, 40(11):907–919, June 2008.

Z. Liu and G. Welsch. Literature survey on diffusivities of oxygen, aluminum, and vanadium in alpha titanium, beta titanium, and in rutile. *Metallurgical and Materials Transactions A*, 19(4):1121–1125, 1988.

A. Majorell, S. Srivatsa, and R. C. Picu. Mechanical behavior of Ti-6Al-4V at high and moderate temperatures–part II: Experimental results. *Materials Science and Engineering A*, 326(2):297–305, 2002.

Savko Malinov, Z. X. Guo, Wei Sha, and A. Wilson. Differential scanning calorimetry study and computer modeling of beta to alpha phase transformation in a ti-6ai-4v alloy. *Metallurgical and Materials Transactions: A*, 32A(4):879, 2001. 10735623.

H. Mecking and Y. Estrin. The effect of vacancy generation on plastic deformation. *Scripta Metallurgica*, 14(7):815, 1980.

H. Mecking and U.F. Kocks. Kinetics of flow and strain-hardening. *Acta Metallurgica*, 29(11):1865–1875, 1981.

Mike Meier and Amiya K. Mukherjee. The strain hardening behavior of superplastic Ti-6Al-4V. *Scripta Metallurgica et Materialia*, 24(2):331, 1990.

Jr Hubert W. Meyer and David S. Kleponis. Modeling the high strain rate behavior of titanium undergoing ballistic impact and penetration. *International Journal of Impact Engineering*, 26(1-10):509–521, 2001.

M. A. Meyers, D.J. Benson, O. Vöhringer, Q. Xue B.K. Kad, and H.-H. Fu. Constitutive description of dynamic deformation: physically-based mechanisms. *Materials Science and Engineering A*, 322(1-2):194–216, 2002.

M. Militzer, W. P. Sun, and J. J. Jonas. Modelling the effect of deformation-induced vacancies on segregation and precipitation. *Acta Metallurgica et Materialia*, 42(1): 133, 1994.

Yuri. Mishin and Chr. Herzig. Diffusion in the Ti-Al system. *Acta Materialia*, 48(3): 589–623, February 2000.

Valentin N. Moiseyev. *Titanium Alloys: Russian Aircraft and Aerospace Applications*, volume 5 of *Advances in Metallic Alloys*. CRC Press, July 2005. ISBN 9780849332739.

F. Montheillet. Dynamic recrystallization: classical concepts and new aspects. *Revue de Metallurgie*, 99(9):767–76, 2002.

D. A. Mosher and P. R. Dawson. A state variable constitutive model for superplastic Ti-6Al-4V based on grain size. *Journal Of Engineering Materials And Technology-Transactions Of The ASME*, 118(2):162–168, 1996.

Sia Nemat-Nasser, Wei-Guo Guo, and J. Y. Cheng. Mechanical properties and deformation mechanisms of a commercially pure titanium. *Acta Materialia*, 47(13): 3705, 1999.

Sia Nemat-Nasser, Wei-Guo Guo, Vitali F. Nesterenko, S. S. Indrakanti, and Ya-Bei Gu. Dynamic response of conventional and hot isostatically pressed Ti-6Al-4V alloys: experiments and modeling. *Mechanics of Materials*, 33(8):425–439, 2001.

P. D. Nicolaou, J. D. Miller, and S. L. Semiatin. Cavitation during hot-torsion testing of Ti-6Al-4V. *Metallurgical and Materials Transactions A*, 36(12):3461, 2005. 10735623.

I. I. Novikov, V. V. Roshchupkin, N. A. Semashko, and L. K. Fordeeva. Experimental investigation of vacancy effects in pure metals. *Journal of Engineering Physics and Thermophysics*, V39(6):1316, 1980.

Eva-Lis Odenberger. *Material characterisation for analyses of titanium sheet metal forming*. Licentiate thesis, Luleå Technical University, 2005.

E Orowan. In *Symposium on Internal Stresses in Metals and Alloys*, page 451. Institute of Metals, 1948.

Chan Hee Park, Young Gun Ko, Jin-Woo Park, and Young Gun Ko. Enhanced superplasticity utilizing dynamic globularization of Ti-6Al-4V alloy. *Materials Science and Engineering: A*, May 2008.

Nho-Kwang Park, Jong-Taek Yeom, and Young-Sang Na. Characterization of deformation stability in hot forging of conventional Ti-6Al-4V using processing maps. *Journal of Materials Processing Technology*, 130-131:540, 2002.

S. Piazolo, M. Jessell, D. J. Prior, and P. D. Bons. The integration of experimental in-situ ebsd observations and numerical simulations: a novel technique of microstructural process analysis. *Journal of Microscopy*, 213(3):273–284, March 2004.

R. C. Picu and A. Majorell. Mechanical behavior of Ti-6Al-4V at high and moderate temperatures–part II: constitutive modeling. *Materials Science and Engineering A*, 326(2):306–316, 2002.

David A. Porter and Kenneth E. Easterling. *Phase Transformations in Metals and Alloys*. CRC Press, 2 edition, 1992. ISBN 9780748757411.

Y. V. R. K. Prasad and S. Sasidhara, editors. *Hot working guide: A compendium of processing maps*. ASM International, 1 edition, May 1997.

Y. V. R. K. Prasad and T. Seshacharyulu. Processing maps for hot working of titanium alloys. *Materials Science and Engineering A*, 243(1-2):82–88, 1998.

Y. V. R. K. Prasad, T. Seshacharyulu, S. C. Medeiros, and W. G. Frazier. A study of beta processing of Ti-6Al-4V: Is it trivial? *Journal of Engineering Materials and Technology*, 123(3):355–360, 2001.

F. Prinz, A. S. Argon, and W. C. Moffatt. Recovery of dislocation structures in plastically deformed copper and nickel single crystals. *Acta Metallurgica*, 30(4): 821–830, 1982.

W. T. Read and W. Shockley. Dislocation models of crystal grain boundaries. *Phys. Rev.*, 78(3):275–289, May 1950. doi: 10.1103/PhysRev.78.275.

Robert E. Reed-Hill and Reza Abbaschian. *Physical Metallurgy Principles*. PWS Publishing Company, 3 edition, 1991. ISBN 0-534-92173-6.

Rolf Sandstrom and Rune Lagneborg. A model for hot working occurring by recrystallization. *Acta Metallurgica*, 23(3):387, 1975.

F. J. Seco and A. M. Irisarri. Creep failure mechanisms of a Ti-6Al-4V thick plate. *Fatigue & Fracture of Engineering Materials and Structures*, 24(11):741, 2001. doi:10.1046/j.1460-2695.2001.00426.x.

Alfred Seeger. The mechanism of glide and work hardening in fcc and hcp metals. In J.C. Fisher, W. G. Johnston, R. Thomson, and T. Jr. Vreeland, editors, *Dislocations and Mechanical Properties of Crystals*, pages 243–329, 1956.

S. Semiatin, S. Knisley, P. Fagin, D. Barker, and F. Zhang. Microstructure evolution during alpha-beta heat treatment of Ti-6Al-4V. *Metallurgical and Materials Transactions A*, 34(10):2377–2386, 2003.

S. L. Semiatin and Thomas R. Bieler. The effect of alpha platelet thickness on plastic flow during hot working of Ti-6Al-4V with a transformed microstructure. *Acta Materialia*, 49(17):3565, 2001.

S. L. Semiatin, V. Seetharaman, and I. Weiss. Hot workability of titanium and titanium aluminide alloys–an overview. *Materials Science and Engineering A*, 243 (1-2):1–24, 1998.

S. L. Semiatin, V. Seetharaman, and A. K. Ghosh. Plastic flow, microstructure evolution, and defect formation during primary hot working of titanium and titanium aluminide alloys with lamellar colony microstructures. *Philosophical Transactions: Mathematical, Physical and Engineering Sciences*, 357:1487 – 1512, 1999.

S. L. Semiatin, N. Stefansson, and R. D. Doherty. Prediction of the kinetics of static globularization of Ti-6Al-4V. *Metallurgical and Materials Transactions*, 36A(5): 1372–1376, 2005.

Songwon Seo, Oakkey Min, and Hyunmo Yang. Constitutive equation for Ti-6Al-4V at high temperatures measured using the shpb technique. 31(6):735, 2005.

T. Seshacharyulu, S. C. Medeiros, W. G. Frazier, and Y. V. R. K. Prasad. Microstructural mechanisms during hot working of commercial grade Ti-6Al-4V with lamellar starting structure. 325(1-2):112, 2002.

J Sheppard and J Norley. Deformation characteristics of Ti-6Al-4V. *Material Science and Technology*, 4(10):903–908, 1988.

Paul G. Shewmon. *Diffusion in solids*. McGraw-Hill series in materials science and engineering. McGraw-Hill, 1963.

J. C. Simo and R. L. Taylor. A return mapping algorithm for plane stress elastoplasticity. *International Journal for Numerical Methods in Engineering*, 22(3):649–670, 1986.

J.C. Simo and T. J. R. Hughes. *Computational Inelasticity*, volume 7 of *Interdisciplinary Applied Mathematics*. Springer, 1 edition, 1998. ISBN 978-0-387-97520-7.

N. Stefansson, S. L. Semiatin, and D. Eylon. The kinetics of static globularization of Ti-6Al-4V. *Metallurgical and Materials Transactions*, 33A(11):3527–3534, 2002. 10735623.

Donald C. Stouffer and L. Thomas Dame. *Inelastic Deformation of Metals: Models, Mechanical Properties, and Metallurgy*. John Wiley & Sons, Inc, February 1996. ISBN 978-0-471-02143-8.

R. Bieler Thomas, P. D. Nicolaou, and S. L. Semiatin. An experimental and theoretical investigation of the effect of local colony orientations and misorientation on cavitation during hot working of Ti-6Al-4V. *Metallurgical and Materials Transactions A*, 36A(1):129, 2005. 10735623.

Jaimie S Tiley. *Modeling of Microstructure Property Relationships in Ti-6Al-4V*. PhD thesis, Ohio State University, 2002.

M. Vanderhasten, L. Rabet, and B. Verlinden. Deformation mechanisms of Ti-6Al-4V during tensile behavior at low strain rate. *Journal of Materials Engineering and Performance*, 16(2):208, 2007. 10.1007/s11665-007-9033-3.

Eva-Lis Westman. Development of an inverse modelling programming system for evaluation of Ti-6Al-4V gleeble experiments. Master's thesis, Luleå University of Technology, 2003.

Jr. William D. Callister. *Materials Science and Engineering: An Introduction*. Wiley, 7 edition, March 2006. ISBN 978-0-471-73696-7.

E. Woldt and D. Juul Jensen. Recrystallization kinetics in copper: Comparison between techniques. *Metallurgical and Materials Transactions A*, 26(7):1717–1724, 1995. 10.1007/BF02670758.

Frank J. Zerilli and Ronald W. Armstrong. Dislocation mechanics based constitutive equation incorporating dynamic recovery and applied to thermomechanical shear instability. In *The tenth American Physical Society topical conference on shock compression of condensed matter*, volume 429, page 215, Amherst, Massachusetts (USA), 1998. AIP.

PAPER I

Dislocation density based constitutive model for Ti-6Al-4V at low strain rates.
Bijish Babu, *Proceedings of the 11th World Conference on Titanium (Ti-2007).*
Kyoto. December-2007. p311-314. ISBN:978-4-88903-406-6

Dislocation density based constitutive model for Ti-6Al-4V at low strain rates

Bijish Babu

Division of Material Mechanics, Luleå University of Technology, Luleå, SE-971 87, Sweden.

This paper summarizes a physically based constitutive model for the mechanical constitutive behavior of Ti-6Al-4V to be used for welding, metal deposition and heat treatment simulations. Dislocation density and vacancy concentration are treated as the internal state variables. Hardening and softening are attributed to the interaction of dislocations with the dislocation substructure and also with vacancies. Dislocation glide and climb are the mechanisms for recovery.

Keywords: *constitutive model, dislocation density, vacancy concentration, flow softening, recovery, dislocation climb, dislocation glide.*

1. Introduction

The plastic behavior of Ti-6Al-4V involves varying phases and textures/morphologies[1,2]. A constitutive model using dislocation density and vacancy concentration as internal state variables can incorporate the complex physics of plasticity. This approach inherently couples macro, micro and sub-micro scales. Parameters of this model are calibrated using standard uniaxial tests and available literature data. Majorell and Picu have used a similar model for Ti-6Al-4V with dislocation density as a single state variable [3, 4)]

2. The Constitutive Model

A simple dislocation density model is described below with the density of immobile dislocations and concentration of vacancies as additional internal variables with separate evolution equations. A model using similar approach is already implemented for manufacturing simulations[5)]. The flow stress is assumed to consist of two parts

$$\sigma_y = \sigma_G + \sigma^* \tag{1}$$

where, σ_G is stress due to long-range interactions with the dislocation substructure. It is an athermal stress contribution. σ^* is the stress due to short-range interactions. It is the friction stress needed to move dislocations through the lattice and to pass short-range obstacles. Thermal vibrations can assist the stress to overcome these obstacles. The long-range term in eq. (1) is written as

$$\sigma_G = m\alpha G b\sqrt{\rho_i} \tag{2}$$

where, m is the Taylor orientation factor translating the effect of the resolved shear stress in different slip systems into effective stress and strain quantities. α is a proportionality factor, ρ_i is the immobile dislocation density, G is the temperature dependent shear modulus and b is the Burger's vector. Different variants of eq. (2) have been used when different dislocations densities are accounted for.

The dislocation velocity is related to the plastic strain rate via the Orowan equation

$$\dot{\bar{\varepsilon}}^p = \frac{\rho_m b \bar{v}}{m} \tag{3}$$

where, $\bar{v}$ is the average velocity of mobile dislocations, ρ_m. This velocity is related to the time taken for a dislocation to pass an obstacle. Here only the waiting time is accounted for since flight time is negligible in comparison. Average velocity can be written as

$$\bar{v} = v_0 \exp(-\Delta G/kT) \;\; = \Lambda \upsilon_a \exp(-\Delta G/kT) \tag{4}$$

where, Λ is the mean free path between two successful events. υ_a is the attempt frequency. ΔG is the activation energy, k is the Boltzmann constant and T is the temperature in Kelvin. Combining eq. (3) and (4) gives

$$\dot{\bar{\varepsilon}}^p = \frac{\rho_m \Lambda b \upsilon_a}{m} \exp(-\Delta G/kT) \tag{5}$$

This equation is rewritten as Ashby and Frost[6])

$$\dot{\bar{\varepsilon}}^p = f\left(\bar{\sigma} - \sigma_G\right)\exp(-\Delta G/kT) \tag{6}$$

where, $\bar{\sigma}$ is the effective stress due to the applied load.

The form of the function f and ΔG depend on the stresses, type of obstacles etc. The stress available to move the dislocation is thus the difference between applied stress and the long-range flow stress component. The effective stress $\bar{\sigma}$ is assumed to be equal to the flow stress σ_y during the deformation. This gives,

$$\sigma^* = \bar{\sigma} - \sigma_G \tag{7}$$

$$\dot{\bar{\varepsilon}}^p = f(\sigma^*)\exp(-\Delta G/kT) \tag{8}$$

The activation energy, can be written as,

$$\Delta G = \Delta F b^3 \left(1 - \left(\frac{\sigma^*}{\sigma_{th}}\right)^p\right)^q \tag{9}$$

$$0 \le p \le 1 \;\; ; \;\; 1 \le q \le 2$$

Some guidelines for choice of ΔF and σ_{th} have been developed by Ashby and Frost[6]). The second term in eq. (1), the short-range stress component can then be written as

$$\sigma^* = \sigma_{th}\left(1-\left(\frac{kT}{\Delta F b^3}\ln\left(\frac{\dot{\varepsilon}_{ref}}{\dot{\varepsilon}^p}\right)\right)^{1/q}\right)^{1/p} \tag{10}$$

The basic ingredients for the yield stress in eq. (1) are obtained from eq. (2) and (12). However, there is a need for an evolution equation for the immobile dislocation density in the eq. (2).

2.1 Evolution of density of immobile dislocations

The basic evolution equations for the immobile dislocation density have two competing parts; storage and recovery.

$$\dot{\rho}_i = \dot{\rho}_i^{(+)} - \dot{\rho}_i^{(-)} \tag{11}$$

2.1.1 Storage

It is assumed that mobile dislocations move a distance (mean free path), Λ before they are immobilized or annihilated. The density of mobile dislocations and their average velocity are related to the plastic strain rate according to the Orowan equation. The increase in the immobile dislocation density is also assumed to be proportional to the plastic strain rate. This leads to[7)]

$$\dot{\rho}_i^{(+)} = \frac{m}{b}\frac{1}{\Lambda}\dot{\varepsilon}^p \tag{12}$$

where *m* is the Taylor orientation factor. The mean free path is written as

$$\frac{1}{\Lambda^2} = \left(\frac{1}{g^2}+\frac{1}{s^2}+\text{others}\right) \tag{13}$$

where, g is grain size, s is dislocation subcell or subgrain diameter, "others" denotes contributions from varying types of obstacles like precipitates or the distance between martensite lathes

Models for recrystallisation and grain growth can be coupled with g and s. The effect of grain size on flow stress, the Hall- Petch relation, is accounted for via this equation and its effect depends on the subcell size or distribution of other dislocation pinning obstacles.

The formation and evolution of subcell is related to the dislocation density by Holt's[8)] relation,

$$s = K_c\frac{1}{\sqrt{\rho_i}} \tag{14}$$

where K_c is a material constant.

2.1.2 Recovery

Recovery is the re-mobilization of the pinned dislocations resulting in a reduction in the flow stress. The two recovery mechanisms considered in this model are dislocation climb and glide.

2.1.2.1 Climb

Dislocations move past obstacles along a direction perpendicular to glide plane by the climb mechanism. This is made possible by the vacancy diffusion process leading to transport of matter. Rate of climb depends on concentration and diffusivity of lattice vacancies which is proportional to self-diffusion rate.

Militzer *et al*.[9)] used a formulation based on Sandström and Lagneborg[10)] and Mecking and Estrin[11)] with a modification of the diffusivity.

$$\dot{\rho}_i^{(-)} = 2D_v^*\frac{Gb^3}{kT}\rho_i^2 = 2D_v\frac{c_v}{c_v^{eq}}\frac{Gb^3}{kT}\rho_i^2 \tag{15}$$

where, c_v^{eq} is the thermal equilibrium vacancy concentration. In the model, immobile dislocation density is adjusted towards an equilibrium limiting value ρ_{eq} as,

$$\dot{\rho}_i^{(-)} = 2c_\gamma D_v\frac{c_v}{c_v^{eq}}\frac{Gb^3}{kT}\left(\rho_i^2-\rho_{eq}^2\right) \tag{16}$$

where, c_γ is a material coefficient.

2.1.2.2 Glide

The glide term of recovery is proportional to immobile dislocation density and the plastic strain rate[5)].

$$\dot{\rho}_i^{(-)} = \Omega\rho_i\dot{\varepsilon}^p \tag{17}$$

where Ω is the glide proportionality factor.

2.2 Evolution of excess vacancies

The relation for the equilibrium concentration of mono-vacancies at a given temperature is[11)],

$$c_v^{eq} = \exp\left(\frac{\Delta S_{vf}}{k}\right)\exp\left(-\frac{Q_{vf}}{kT}\right) = c_{v0}\exp\left(-\frac{Q_{vf}}{kT}\right) \tag{18}$$

where, Q_{vf} is the activation energy for vacancy formation and ΔS_{vf} is the entropy increase during vacancy formation. The self-diffusion coefficient can be written as

$$D_v = a^2 \upsilon \exp(\frac{\Delta S_{vm} + \Delta S_{vf}}{k}) \exp(-\frac{Q_{vm} + Q_{vf}}{kT}) = D_{v0} \exp(-\frac{Q_v}{kT}) \quad (19)$$

where a is the lattice constant, υ is the lattice vibration frequency, ΔS_{vm} is the entropy increase and Q_{vm} is the energy barrier for migration of an atom to a vacancy. The self-diffusivity can be written as

$$D_v = c_v^{eq} a^2 \upsilon \exp(\frac{\Delta S_{vm}}{k}) \exp(-\frac{Q_{vm}}{kT}) \quad (20)$$

Thus the self-diffusivity is proportional to the equilibrium concentration of vacancies. Self-diffusivity for any non-equilibrium vacancy concentration can be written as,

$$D_v^* = \frac{c_v}{c_v^{eq}} D_v \quad (21)$$

Vacancy migration results in vacancy annihilation. Migration of vacancies is attributed to self-diffusion of existing vacancies. Thus it is written as

$$D_{vm} = a^2 \upsilon \exp(\frac{\Delta S_{vm}}{k}) \exp(-\frac{Q_{vm}}{kT}) = D_{vm0} \exp(-\frac{Q_{vm}}{kT}) \quad (22)$$

Militzer[9] used a model for vacancy concentration as below.

$$\dot{c}_v^{ex} = \dot{c}_v - \dot{c}_v^{eq} = \left[\chi \frac{\sigma b}{Q_{vf}} + \varsigma \frac{c_j}{4b^2} \right] \frac{\Omega_0}{b} \dot{\bar{\varepsilon}} - D_{vm} \left(\frac{1}{s^2} + \frac{1}{g^2} \right) \left(c_v - c_v^{eq} \right) \quad (23)$$

where, $\chi \approx 0.1$ is the fraction of mechanical energy spent on vacancy generation, ς is the neutralization effect by vacancy emitting and absorbing jogs.

$$\varsigma = \begin{cases} 0.5 - \varsigma_0 c_j & \text{if } c_j \le 0.5/\varsigma_0 \\ 0 & \text{if } c_j > 0.5/\varsigma_0 \end{cases} \quad (24)$$

c_j is the concentration of jogs given by

$$c_j = \exp(-\frac{Q_{fj}}{kT}) \quad (25)$$

Q_{fj} is the formation energy approximated as

$$Q_{fj} = \frac{Gb^3}{4\pi(1-\nu)} \quad (26)$$

Ω_0 is the atomic volume and c_v^{eq} is the equilibrium concentration of vacancies. Assuming that only long range stress contributes to vacancy formation, $\sigma_y = \sigma_G$ and substituting the mean free path, Millitzer equation[9] can be rewritten as

$$\dot{c}_v^{ex} = \left(\chi \frac{m \alpha G b^2}{Q_{vf}} \sqrt{\rho_i} + \varsigma \frac{c_j}{4b^2} \right) \frac{\Omega_0}{b} \dot{\bar{\varepsilon}} - D_{vm} \left(\frac{1}{\Lambda^2} \right) \left(c_v - c_v^{eq} \right) \quad (27)$$

3. Solution of evolution equations for internal variables

The internal variables are

$$\mathbf{q} = \begin{bmatrix} \rho_i \\ c_v \end{bmatrix} \quad (28)$$

The state variables are expressed as a coupled set of differential equations and are solved by a Newton iterative procedure.

The hardening modulus is defined as,

$$\mathbf{H}_{(i)} = 0 \quad (29)$$

$$H_1 = \Delta q_1 - \left[\frac{m}{b\Lambda} \Delta \bar{\varepsilon}^p - \Omega q_1 \Delta \bar{\varepsilon}^p - 2 c_\gamma D_v q_2 \frac{Gb^3}{kT} \left(q_1^2 - \rho_{eq}^{\ 2} \right) \rho_{i0} \Delta t \right] = 0 \quad (30)$$

$$H_2 = \Delta q_2 - \left[\chi \frac{\Omega_0 m \alpha G b}{Q_{vf}} \sqrt{q_1} \Delta \bar{\varepsilon}^p + \varsigma \frac{c_j}{4b^2} \frac{\Omega_0}{b} \Delta \bar{\varepsilon}^p - \frac{D_{vm}}{\Lambda^2} \left(q_2 - c_v^{eq} \right) \Delta t + \left(\frac{Q_{vf}}{T^2} \right) \Delta T \right] = 0 \quad (31)$$

$$dq = -\left[\frac{\partial \mathbf{H}}{\partial \mathbf{q}} \right]^{-1} \cdot \mathbf{H} \quad (32)$$

$$q^{n+1} = q^n + dq^{n+1} \quad (33)$$

Derivatives of the hardening modulus can be written as below.

$$\frac{\partial H_1}{\partial q_1} = 1 + \Omega q_1 \Delta \bar{\varepsilon}^p + 4 c_\gamma D_v q_2 \frac{Gb^3}{kT} q_1 \Delta t \quad (34)$$

$$\frac{\partial H_1}{\partial q_2} = 2c_\gamma D_v \frac{Gb^3}{kT}\left(q_1^2 - \rho_{eq}^2\right)\Delta t \tag{35}$$

$$\frac{\partial H_2}{\partial q_1} = -0.5\chi \frac{\Omega_0 m\alpha Gb}{Q_{vf}\sqrt{q_1}}\Delta\bar{\varepsilon}^p \tag{36}$$

$$\frac{\partial H_2}{\partial q_2} = 1 + \frac{D_{vm}}{\Lambda^2}\Delta t \tag{37}$$

4. Material Testing

Isothermal compression test at strain rates of $0.001s^{-1}$ has been conducted on cylindrical specimens of Ti6Al-4V. The chemical composition of the material is shown in the table below.

Table 1. Plate material composition; remaining is Ti

Al	V	O	Fe	Mo	C	Si	Mn	H
6.19	3.98	0.1620	0.21	<0.01	0.010	<0.01	<0.01	0.0082

5. Results and Discussion

The computed model and compression test data are presented in the Figure 1. The results from testing are smoothed to remove the fluctuations from machine error. Also the compliance of the testing equipment is removed from the results based on the previous experience.

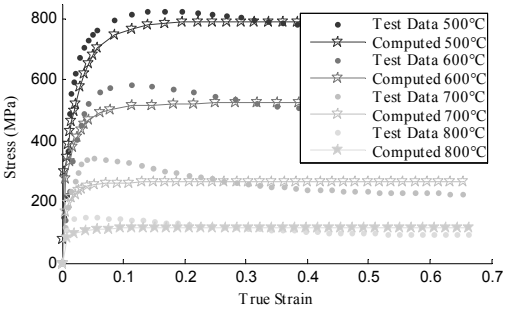

Figure 1. Comparison of computed and tested data

The parameters of the model are presented in the table 2 and 3.

6. Conclusions

This model provides a bridge between different length scales. Ti-6Al-4V undergoes dynamic recrystallisation at elevated temperatures. But current model is incapable of simulating this phenomenon.

Acknowledgement

This work has been performed in the VERDI project under the 6th frame work program of the European Commission and the author wish to thank the VERDI consortium for providing financial support.

Table 2. Parameters for the model (temperature dependant)

T(°C)	500	600	700	800
E (MPa)	78400	66000	43700	23300
α	5.0	4.40	4.50	4.25
Ω_0	45	52	80	100

Table 3. Parameters for the model (temperature independent)

υ	c_γ	K_c	s_∞	τ_0	Δf_0	p	q	ρ_{i0}	ρ_{eq}	$\dot{\bar{\varepsilon}}_{ref}$
			m					m/m^3		s^{-1}
0.3	0.5	50	$1e^{-6}$	0.5	0.3	0.7	2.7	$1e^{13}$	$1e^{10}$	$1e^{7}$

REFERENCES

1) Thomas, R.B., P.D. Nicolaou, and S.L. Semiatin, An Experimental and Theoretical Investigation of the Effect of Local Colony Orientations and Misorientation on Cavitation during Hot Working of Ti-6Al-4V. Metallurgical and Materials Transactions A, 2005. 36A(1): p. 129.

2) Semiatin, S.L., Seetharaman. V, Ghosh, A. K., Plastic flow, microstructure evolution, and defect formation during primary hot working of titanium and titanium aluminide alloys with lamellar colony microstructures. Philosophical Transactions: Mathematical, Physical and Engineering Sciences, 1999. 357: p. 1487 - 1512.

3) Majorell, A., S. Srivatsa, and R.C. Picu, Mechanical behavior of Ti-6Al-4V at high and moderate temperatures--Part I: Experimental results. Materials Science and Engineering A, 2002. 326(2): p. 297-305.

4) Picu, R.C. and A. Majorell, Mechanical behavior of Ti-6Al-4V at high and moderate temperatures--Part II: constitutive modeling. Materials Science and Engineering A, 2002. 326(2): p. 306-316.

5) Domkin, K., Constitutive models based on dislocation density: formulation and implementation into finite element codes, in Department of Applied Physics and Mechancal Engineering, Division of CAD. 2005, Luleå Technical Univeristy: Luleå. p. 168.

6) Frost, H.J. and M.F.A. FRS, Deformation-Mechanism Maps: The Plasticity and Creep of Metals and Ceramics. 1982: Paperback.

7) Estrin, Y., Dislocation theory based constitutive modelling: foundations and applications. Journal of Materials Processing Technology, 1998. 80-81): p. 33.

8) Holt, D.L., Dislocation cell formation in metals. Journal of Applied Physics. 1970, Volume-41, No. 8.

9) Militzer, M., W.P. Sun, and J.J. Jonas, Modelling the effect of deformation-induced vacancies on segregation and precipitation. Acta Metallurgica et Materialia, 1994. 42(1): p. 133.

10) Sandstrom, R. and R. Lagneborg, A model for hot working occurring by recrystallization. Acta Metallurgica, 1975. 23(3): p. 387.

11) Mecking, H. and Y. Estrin, The effect of vacancy generation on plastic deformation. Scripta Metallurgica, 1980. 14(7): p. 815.

PAPER II

Dislocation density based constitutive model for Ti-6Al-4V: including recovery and recrystallisation. Bijish Babu, *Computational plasticity: Fundamentals and Applications (COMPLAS IX)*. Barcelona. September-2007. p631-634.
ISBN:978-84-96736-29-0

IX International Conference on Computational Plasticity
COMPLAS IX
E. Oñate and D. R. J. Owen (Eds)

DISLOCATION DENSITY BASED CONSTITUTIVE MODEL FOR TI-6AL-4V: INCLUDING RECOVERY AND RECRYSTALLISATION

Bijish Babu

Luleå University of Technology
Luleå, SE-977 51, Sweden
E-mail: bijish.babu@ltu.se, web page: http://www.ltu.se

Key words: Dislocation Density, Vacancy, Grain Size, Recovery, Recrystallisation

1 INTRODUCTION

This paper investigates the plastic deformation of Ti-6Al-4V at low strain rates and high temperatures. The dependence of flow stress on temperature and strain rate is investigated. Ti-6Al-4V exhibits pronounced flow softening behavior at elevated temperature[1]. Possible mechanisms responsible for this behavior are discussed and a physically based constitutive model is developed. Detailed derivations of the equations can be found there.

2 THE CONSTITUTIVE MODEL

A simple dislocation density model is described below with the density of immobile dislocations and concentration of vacancies as additional internal variables with separate evolution equations. A similar model has been developed for AISI-316L. Detailed derivations of equations can be found there[2].

The flow stress is assumed to consist of two parts

$$\sigma_y = \sigma_G + \sigma^* \qquad (1)$$

where, σ_G is stress due to long-range interactions with the dislocation substructure. It is an athermal stress contribution. σ^* is the stress due to short-range interactions. It is the friction stress needed to move dislocations through the lattice and to pass short-range obstacles. Thermal vibrations can assist the stress to overcome these obstacles. The long-range term in eq. (1) is written as

$$\sigma_G = m\alpha Gb\sqrt{\rho_i} \qquad (2)$$

where, m is the Taylor orientation factor translating the effect of the resolved shear stress in different slip systems into effective stress and strain quantities. α is a proportionality factor, ρ_i is the immobile dislocation density, G is the temperature dependent shear modulus and b is the Burger's vector. The second term in eq. (1), the short-range stress component can then be written as

$$\sigma^* = \sigma_{th}\left(1-\left(\frac{kT}{\Delta F b^3}\ln\left(\frac{\dot{\bar{\varepsilon}}_{ref}}{\dot{\bar{\varepsilon}}^{p}}\right)\right)^{1/q}\right)^{1/p} \qquad (3)$$

where, σ_{th} is the athermal flow strength, ΔF is the total free energy, k is the Boltzmann constant and T is the temperature in Kelvin. The basic ingredients for the yield stress in eq. (1) are obtained from eq. (2) and (3). However, there is a need for an evolution equation for the immobile dislocation density in the eq. (2).

2.1 Evolution of density of immobile dislocations

The basic evolution equation for the immobile dislocation density has three components; storage/strain hardening, dynamic recovery and dynamic recrystallisation.

$$\dot{\rho}_i = \dot{\rho}_i^{(+)} - \dot{\rho}_i^{(-)} \quad (4)$$

2.1.1 Storage

It is assumed that mobile dislocations move a distance (mean free path), Λ before they are immobilized or annihilated. The density of mobile dislocations and their average velocity are related to the plastic strain rate according to the Orowan equation. The increase in the immobile dislocation density is also assumed to be proportional to the plastic strain rate. This leads to

$$\dot{\rho}_i^{(+)} = \frac{m}{b}\frac{1}{\Lambda}\dot{\bar{\varepsilon}}^{p}; \quad \frac{1}{\Lambda^2} = \left(\frac{1}{g^2}+\frac{1}{s^2}+\text{others}\right) \qquad (5)$$

where m is the Taylor orientation factor, g is grain size, s is dislocation subcell or subgrain diameter, "others" denotes contributions from varying types of obstacles like precipitates or the distance between martensite lathes. Models for recrystallisation and grain growth can be coupled with g and s. The effect of grain size on flow stress, the Hall- Petch relation, is accounted for via this equation and its effect depends on the subcell size or distribution of other dislocation pinning obstacles.

$$s = \left[K_c - A \;\; K_{DRx}\right]\frac{1}{\sqrt{\rho_i}} \qquad (6)$$

where K_c and K_{DRx} are material constants, $A(\rho_i, \rho_{cr})$ is the activation function and ρ_{cr} is the critical dislocation density. Critical dislocation density is the a function of strain rate and temperature and initiates Dynamic Recrystallisation (DRx)

2.1.2 Recovery

Recovery is the re-mobilization of the pinned dislocations resulting in a reduction in the flow stress. The two recovery mechanisms considered in this model are dislocation climb and glide.

2.1.2.1 Climb

Dislocations move past obstacles along a direction perpendicular to glide plane by the climb mechanism. This is made possible by the vacancy diffusion process leading to transport of matter. Rate of climb depends on concentration and diffusivity of lattice vacancies which is proportional to self-diffusion rate. In the model, immobile dislocation density is adjusted towards an equilibrium limiting value ρ_{eq} as,

$$\dot{\rho}_i^{(-)} = 2c_\gamma D_v \frac{c_v}{c_v^{eq}} \frac{Gb^3}{kT}\left(\rho_i^2 - \rho_{eq}^2\right) \qquad (7)$$

where, c_γ is a material coefficient, c_v^{eq} is the thermal equilibrium vacancy concentration.

2.1.2.2 Glide

The glide term of recovery is proportional to immobile dislocation density and the plastic strain rate.

$$\dot{\rho}_i^{(-)} = \Omega \rho_i \dot{\bar{\varepsilon}}^p \qquad (8)$$

where Ω is the glide proportionality factor.

2.1.3 Dynamic Recrystallisation

Dynamic Recrystallisation occurs during straining of metals at elevated temperatures. It is characterized by formation of new grains with lower dislocation densities. New grains are formed at the expense of the stored dislocations and subcells.

$$\dot{\rho}_i^{(-)} = \Psi A f\left(\rho_i, \Delta\bar{\varepsilon}^p\right) \qquad (9)$$

2.2 Evolution of excess vacancies

Militzer used a model for concentration of excess vacancies as below.

$$\dot{c}_v^{ex} = \dot{c}_v - \dot{c}_v^{eq} = \left[\chi \frac{\sigma b}{Q_{vf}} + \varsigma \frac{c_j}{4b^2}\right] \frac{\Omega_0}{b} \dot{\bar{\varepsilon}} - D_{vm}\left(\frac{1}{s^2} + \frac{1}{g^2}\right)\left(c_v - c_v^{eq}\right) \qquad (10)$$

where, $\chi \approx 0.1$ is the fraction of mechanical energy spent on vacancy generation, ς is the neutralization effect by vacancy emitting and absorbing jogs.

$$\varsigma = \begin{cases} 0.5 - \varsigma_0 c_j & \text{if } c_j \le 0.5/\varsigma_0 \\ 0 & \text{if } c_j > 0.5/\varsigma_0 \end{cases}; \quad c_j = \exp(-\frac{Q_{fj}}{kT}); \quad Q_{fj} = \frac{Gb^3}{4\pi(1-\nu)} \qquad (11)$$

c_j is the concentration of jogs, Q_{fj} is the formation energy and Ω_0 is the atomic volume. Assuming that only long range stress contributes to vacancy formation, $\sigma_y = \sigma_G$ and substituting the mean free path, eq. (11) can be rewritten as

$$\dot{c}_v^{ex} = \left(\chi \frac{m\alpha Gb^2}{Q_{vf}} \sqrt{\rho_i} + \varsigma \frac{c_j}{4b^2} \right) \frac{\Omega_0}{b} \dot{\bar{\varepsilon}} - D_{vm} \left(\frac{1}{\Lambda^2} \right) \left(c_v - c_v^{eq} \right) \qquad (12)$$

3 RESULTS

Isothermal compression test at strain rates of $0.001s^{-1}$ has been conducted on cylindrical specimens of Ti6Al-4V. The computed model and compression test data are presented in the Figure 1. The results from testing are smoothed to remove the fluctuations from machine error. Also the compliance of the testing equipment is removed from the results based on the previous experience.

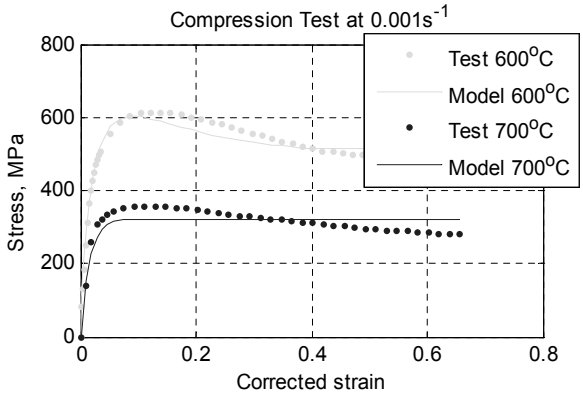

Figure 1: Comparison of Computed and Tested Data

REFERENCES

[1] Semiatin, S.L. *etal*, "Plastic flow, microstructure evolution, and defect formation during primary hot working of titanium and titanium aluminide alloys with lamellar colony microstructures". Philosophical Transactions: Mathematical, Physical and Engineering Sciences, 1999. 357: p. 1487 - 1512.

[2] L-E Lindgren, K Domkin, S Hansson, "Dislocations, Vacancies, and Solute Diffusion Dislocations, Vacancies, and Solute Diffusion in Physical Based Plasticity Model for AlSl 316L", Submitted for publication

PAPER III

Physically based model for plasticity and creep of Ti-6Al-4V. Bijish Babu.
Submitted to the Journal; Mechanics of Materials. October-2008

Physically Based Model for Plasticity and Creep of Ti-6Al-4V

Bijish Babu

Division of Material Mechanics, Luleå University of Technology, SE-971 87, Luleå, Sweden, Tel:+46 920 491824, Fax:+46 920 492228

Abstract

Albeit Ti-6Al-4V has numerous salient properties, its usage for certain applications is limited due to the challenges faced during manufacturing. Understanding the dominant deformation mechanisms and numerically modelling the process is the key to overcome this hurdle. This paper investigates plastic deformation of the alloy at strain rates from $0.001s^{-1}$ to $1s^{-1}$ and temperatures between 20°C and 1100°C. Pertinent deformation mechanisms of the material when subjected to thermo-mechanical processing is discussed. A physically founded constitutive model based on the evolution of immobile dislocation density and excess vacancy concentration is developed. Parameters of the model are obtained by calibration using isothermal compression tests. Model is compared with relaxation test data to demonstrate its validity.

Key words: Dislocation density, Vacancy concentration, Glide, Self Diffusion, Climb, Stress relaxation.

1. Introduction

Ti-6Al-4V has good specific strength, toughness and corrosion resistance which makes it attractive for applications in aerospace, pressure vessels, surgical implants etc. Components for these applications have precise requirements on mechanical and physical properties (James and Lutjering, 2003). Besides, this alloy has a narrow temperature and strain rate window of workability (Kailas et al., 1994; Seshacharyulu et al., 2002). Optimization of the process parameters to satisfy the requirements on the component can be enabled by simulation. This work is part of a project aimed to perform finite element simulations of a manufacturing processes chain involving hot-forming, welding, metal deposition and heat treatment of Ti-6Al-4V components.

Manufacturing process chain simulations can compute the cumulative effect of the various processes by following the material state through the whole chain and give a realistic prediction of the final component. Capacity to describe material behavior in a wide range of temperatures and strain rates is crucial for this task. Such a model should be based on the physical behavior of the material. This paper explains adaptation of a physically based constitutive model for 316L Steel proposed by Lindgren et al. (2008) to Ti-6Al-4V. Similar models have been proposed by Nemat-Nasser et al. (1999) for commercially pure Ti and Picu and Majorell (2002) for Ti-6Al-4V with the exception of the effects of vacancy formation and its evolution.

Dislocation glide controlled by Peierls-Nabarro stress and dislocation climb controlled by lattice and core diffusion are identified as the dominant deformation mechanisms of this alloy. At low temperature ($< 0.5T_{melt}$), the self diffusivity of the alloy is enhanced by the short circuit pipe diffusion. This work extends the Lindgren et al. (2008) model by including the effects of enhanced diffusivity. Additionally, the capacity of the model to simulate diffusion assisted deformation mechanisms responsible for creep and stress relaxation are illustrated in this paper.

2. Material and deformation mechanisms

Ti-6Al-4V is a two phase alloy containing 6wt% Al stabilizing α phase which has HCP structure and 4wt% V stabilizing the β phase which has BCC structure. The proportion of these alloying elements gives attractive mechanical properties to the material. The presence of Al inhibits twinning even though it is a common deformation mechanism for HCP materials (Majorell et al., 2002). The two phases in the alloy have different properties given by their structures, with α exhibiting greater strength yet lower ductility and formability

Email address: bijish.babu@ltu.se (Bijish Babu)
URL: http://mm.project.ltu.se (Bijish Babu)

compared to β phase (Tiley, 2002). The microstructure at equilibrium in room temperature consists mainly of α phase ($\approx$ 95%) with some retained β phase. At around 890°C, the α phase transforms to β. This temperature (β-transus) depends on the composition of Al and V.

The material used in this work was supplied as 12mm thick plates by ATI Allvac®, USA. It is checked for defects using ultrasonic technique and has undergone annealing heat treatment for 6h at 790°C. The material is free from the hard and brittle α-case (oxygen rich surface layer). Cylindrical specimens machined from the plates were used in the experiments. The axis of the specimens are oriented in the transverse direction of rolling. Mechanical properties of Ti-6Al-4V is dependant on different parameters like thermo-mechanical processing, chemical composition, interstitial impurities etc. The chemical composition of the material is shown in table 1. Low-temperature ($< 0.3T_{melt}$) plas-

Table 1: Chemical composition given in wt%. Remaining is Ti.

Al	V	O	Fe	C	Si	Mn	H
6.19	3.98	0.162	0.21	0.01	<0.01	<0.01	0.0082

ticity in Ti-6Al-4V is extremely sensitive to the concentration of interstitial solutes (de Meester et al., 1975). At low temperature, interstitial solutes concentration (C_s) control the plastic flow whereas at higher temperature, it is the concentration of interstitial impurities (C_i) that has control (Conrad, 1981). Studying the effect of strain (ε), strain rate ($\dot{\varepsilon}$), temperature (T) and grain size (g) on Ti systems, Conrad arrived at the following additive strengthening relationship.

$$\sigma = \sigma_G(G, \varepsilon, g, C_s) + \sigma^*(T, \dot{\varepsilon}, C_i) \qquad (1)$$

Here, first component varies with temperature through the temperature dependence of the shear modulus (G). The underlying mechanism of plastic flow is identified as dislocation motion by glide and climb which is assisted by diffusion (Conrad, 1981). The mechanism of diffusion in Ti systems is less understood. The published diffusion data shows large scatter which is attributed to the variation in measurement techniques(Liu and Welsch, 1988; Mishin and Herzig, 2000). Semiatin et al. (2003) measured the diffusivity of Al and V in β-Ti between 700 and 950°C. It has been reported that dislocations in Ti-6Al-4V act as high diffusivity paths leading to an enhanced diffusion (Park et al., 2008).

3. Experiments

Isothermal compression tests at temperatures from 20°C to 1100°C and strain rates from $0.001s^{-1}$ to $1.0s^{-1}$ are performed for calibration of the material model. The length to diameter ratio of the specimen is varied for each temperature to receive a measurable force response from the Gleeble® thermo-mechanical simulator. In order to reduce the friction between the specimen and anvil, Tantalum films were placed in between. In-spite of this, all specimens exhibited barreling which is the evidence for significant friction. The specimens are heated to test temperature at a rate of $10°Cs^{-1}$. It is held for 30s to achieve an even temperature distribution followed by compression at a given strain rate. Finally, they are cooled to room temperature at a rate of $20°Cs^{-1}$.

During compression, force and temperature are controlled using a closed loop control system and longitudinal strain is measured from the displacement of the anvils. Temperature loading is done by resistance electrical heating. However, due to the adiabatic heating, temperature of the specimen increases slightly (< 10°C) during deformation and is recorded with the thermocouple welded to the specimen. Diametrical change of the specimen is measured during the tests. This data combined with the force measurement from the load cell is used to compute the stress. The data obtained from measurement is smoothed to remove the noise generated by the dynamics of the machine operation. Also, corrections are made to adjust the compliance of the anvil and lubricant film.

Since the specimens were cut from plates, it exhibited strong anisotropy of the mechanical properties which was evident from the ovality after deformation. However this was ignored in the calculations. Owing to the strong affinity of the alloy to oxygen at high temperatures, the experiments were performed in an evacuated chamber.

4. Formulation of the flow stress model

The flow stress model is formulated on a homogeneous representative volume element and it provides a bridge between various sub-micro scale phenomena and macro scale continuum mechanics. Properties of dislocations are related to macroscopic plasticity. Plastic strain is associated to motion of dislocations, while hardening or softening is associated to interaction of dislocations. With the increase of dislocation density, the dislocations themselves get entangled and prevent further motion which results in isotropic hardening.

Due to the lattice distortion from plastic deformation, elastic energy is stored in the material which also hinders the movement of the dislocations leading to kinematic hardening. However, the internal stresses support dislocation movement in the opposite direction resulting in the so called "Bauschinger effect". Recovery and recrystallization are two competing restoration mechanisms and they balance the strain hardening. In order to compute evolution of the material state, dislocation density and vacancy concentration are used as internal state variables in this model.

4.1. Flow Stress

The flow stress is assumed to consist of two parts (Seeger, 1956; Bergström, 1969; Kocks, 1976),

$$\sigma_y = \sigma_G + \sigma^* \tag{2}$$

where, σ_G is the athermal stress contribution from the long-range interactions of the dislocation substructure. The second term σ^*, is the friction stress needed to move dislocations through the lattice and to pass short-range obstacles. Thermal vibrations can assist dislocations to overcome these obstacles. This formulation is very much in accordance to the material behavior demonstrated by Conrad (1981) in equation (1).

Long range stress component:
The long-range term from equation (2) is derived by Seeger (1956) as,

$$\sigma_G = m\alpha G b \sqrt{\rho_i} \tag{3}$$

where m is the Taylor orientation factor translating the effect of the resolved shear stress in different slip systems into effective stress and strain quantities. Furthermore, α is a proportionality factor, b is the Burger's vector and ρ_i is the immobile dislocation density. The shear modulus can be computed from the Youngs modulus (E) and Poisson ratio (ν) as,

$$G = \frac{E}{2(1+\nu)} \tag{4}$$

Short range stress component:
The dislocation velocity is related to plastic strain rate via the Orowan equation (Orowan, 1948)

$$\dot{\varepsilon}^p = \frac{\rho_m b \bar{v}}{m} \tag{5}$$

where $\bar{v}$ is the average velocity of mobile dislocations (ρ_m). This velocity is related to the time taken by a dislocation to pass an obstacle most of which is the waiting time. The velocity is written according to Frost and Ashby (1982) as,

$$\bar{v} = \Lambda \nu_a e^{-\Delta G/kT} \tag{6}$$

where Λ is the mean free path, ν_a is the attempt frequency, ΔG is the activation energy, k is the Boltzmann constant and T is the temperature in Kelvin. Here, $e^{-\Delta G/kT}$ can be considered as the probability that the activation energy is supplied locally.

$$\dot{\bar{\varepsilon}}^p = f e^{-\Delta G/kT} \tag{7}$$

The form of the function f and ΔG depend on the applied stress, strength of obstacles etc. The stress available to move a dislocation past an obstacle is the difference between applied stress and the long-range flow stress component. Since the effective stress during plasticity is equal to the flow stress, $f = f(\bar{\sigma} - \sigma_G) = f(\sigma^*)$. The activation energy can be written according to Kocks et al. (1975) as,

$$\Delta G = \Delta F \left[1 - \left(\frac{\sigma^*}{\sigma_{ath}} \right)^p \right]^q \tag{8}$$
$$0 \le p \le 1$$
$$1 \le q \le 2$$

Here, $\Delta F = \Delta f_0 G b^3$ is the activation energy necessary to overcome lattice resistance and $\sigma_{ath} = \tau_0 G$ is the shear strength in the absence of thermal energy. Some guidelines for selection of Δf_0 and τ_0 are given in Table 2. Here l is the mean spacing of the obstacles; either precipitates or solutes. The strain rate dependent part of the yield stress from equation (2) can be derived according to the Kocks-Mecking formulation (Kocks et al., 1975; Mecking and Kocks, 1981) as,

Table 2: Activation energy factor and shear strength of different obstacles from Frost and Ashby (1982).

Obstacle Strength	Δf_0	τ_0	Example
Strong	2	$> \frac{b}{l}$	Strong precipitates
Medium	0.2 – 1.0	$\approx \frac{b}{l}$	Weak precipitates
Weak	< 0.2	$\ll \frac{b}{l}$	Lattice Resistance,

$$\sigma^* = \tau_0 G \left[1 - \left[\frac{kT}{\Delta f_0 G b^3} \ln \left(\frac{\dot{\varepsilon}^{ref}}{\dot{\bar{\varepsilon}}^p} \right) \right]^{1/q} \right]^{1/p} \tag{9}$$

Here $\dot{\varepsilon}^{ref}$ is the reference strain rate.

4.2. Evolution of immobile dislocation density

The basic components for the yield stress in equation (2) are obtained from equations (3 and 9). However, the evolution of ρ_i in equation (3) needs to be computed. The model for evolution of the immobile dislocation density has two parts; hardening and restoration.

$$\dot{\rho}_i = \dot{\rho}_i^{(+)} + \dot{\rho}_i^{(-)} \tag{10}$$

4.2.1. Hardening Process

It is assumed that mobile dislocations move, on average, a distance Λ (mean free path), before they are immobilized or annihilated. According to the Orowan equation, density of mobile dislocations and their average velocity are proportional to the plastic strain rate. It is reasonable to assume that increase in immobile dislocation density also follow the same relation. This leads to,

$$\dot{\rho}_i^{(+)} = \frac{m}{b}\frac{1}{\Lambda}\dot{\bar{\varepsilon}}^p \tag{11}$$

where m is the Taylor orientation factor. The mean free path can be computed from the grain size (g) and dislocation subcell or subgrain diameter (s) as,

$$\frac{1}{\Lambda} = \left(\frac{1}{g} + \frac{1}{s} + others\right) \tag{12}$$

where *others* denote contributions from obstacles like precipitates, interstitial elements, martensite lathes etc. Models for recrystallization, grain growth, precipitation, dissolution etc can be included here. The effect of grain size on flow stress known as Petch-Hall relation, is accounted via this term.

The formation and evolution of subcells has been modelled using a relation proposed by Holt (1970) with s_∞ as the minimum subcell size.

$$s = K_c\frac{1}{\sqrt{\rho_i}} + s_\infty \tag{13}$$

4.2.2. Restoration Processes

Motion of vacancies is related to recovery of dislocations. This occur usually at elevated temperatures and therefore is a thermally activated reorganization process. Creation of vacancy increases entropy but consumes energy and its concentration increases with temperature and deformation. In high stacking fault materials, recovery process might balance the effects of strain hardening leading to a constant flow stress.

Recovery by Glide:
Kocks et al. (1975) has derived an equation for evolution of mobile dislocation density which can be written as,

$$\dot{\rho}_m = \rho_m\bar{\nu}\left(\frac{1}{\Lambda_{back}} - \frac{1}{\Lambda}\right) \tag{14}$$

where, Λ_{back} is the distance travelled by a previously emitted dislocation and $\bar{\nu}$ is the spacial average velocity of mobile dislocations.

Based on the formulation by Bergström (1983), the immobile dislocation density is propotional to the plastic strain rate.

$$\dot{\rho}_i^{(-)} = \Omega\rho_i\dot{\bar{\varepsilon}}^p \tag{15}$$

where Ω is a function dependent on temperature. This is analogous to Kocks formulation as ρ_i and $\dot{\bar{\varepsilon}}^p$ are proportional to ρ_m and $\bar{\nu}$ respectively.

Recovery by Climb:
In addition to dislocations, vacancies are also created during plastic deformation (Fridel, 1964). This has significant effect on diffusion controlled processes such as climb and dynamic strain ageing. Militzer et al. (1994) proposed a model based on Sandstrom and Lagneborg (1975) and Mecking and Estrin (1980). With a modification of the diffusivity according to equation (25), this can be written as,

$$\dot{\rho}_i^{(-)} = 2c_\gamma D_l\frac{c_v}{c_v^{eq}}\frac{Gb^3}{kT}\left(\rho_i^2 - \rho_{eq}^2\right) \tag{16}$$

where, c_v^{eq} and c_v are equilibrium and current vacancy concentrations and c_γ, a material coefficient.

4.3. Evolution of excess vacancy concentration

The concentration of vacancies attain equilibrium if left undisturbed in isothermal conditions. When subjected to deformation or temperature change, the material generates excess vacancies. The model considered here is only concerned with mono-vacancies. The equilibrium concentration of vacancies at a given temperature according to **?**Reed-Hill and Abbaschian (1991) is

$$c_v^{eq} = e^{\frac{\Delta S_{vf}}{k}}e^{-\frac{Q_{vf}}{kT}} \tag{17}$$

where, ΔS_{vf} is the increase in entropy while creating a vacancy and Q_{vf} is the activation energy for vacancy formation.

Vacancy Creation and Annihilation:
Militzer et al. (1994) proposed a model for excess

vacancy concentration with generation and annihilation components as,

$$\dot{c_v}^{ex} = \dot{c}_v - \dot{c}_v^{eq} = \left[\chi \frac{\sigma b}{Q_{vf}} + \zeta \frac{c_j}{4b^2}\right] \frac{\Omega_0}{b} \bar{\varepsilon} - D_{vm} \left[\frac{1}{s^2} + \frac{1}{g^2}\right] \left(c_v - c_v^{eq}\right) \quad (18)$$

Here, $\chi = 0.1$ is the fraction of mechanical energy spent on vacancy generation, Ω_0 is the atomic volume and ζ is the neutralization effect by vacancy emitting and absorbing jogs which is computed as below.

$$\zeta = \begin{cases} 0.5 - \zeta_0 c_j & if\ c_j \leq 0.5/\zeta_0 \\ 0 & if\ c_j > 0.5/\zeta_0 \end{cases} \qquad \zeta_0 = 10 \quad (19)$$

The concentration of jogs is given as,

$$c_j = e^{-\frac{Q_{jf}}{kT}}; \quad Q_{jf} = \frac{Gb^3}{4\pi(1-\nu)}$$

where Q_{jf} is the activation energy of jog formation.

Assuming that only long range stress contributes to vacancy formation and introducing mean free path, equation (18) becomes,

$$\dot{c_v}^{ex} = \left[\chi \frac{m\alpha G b^2}{Q_{vf}} + \zeta \frac{c_j}{4b^2}\right] \frac{\Omega_0}{b} \bar{\varepsilon} - D_{vm} \left[\frac{1}{\Lambda^2}\right] \left(c_v - c_v^{eq}\right) \quad (20)$$

Vacancy Creation from Temperature Change:
Additionally, excess vacancy concentration can be driven by temperature change as,

$$\dot{c_v}^{ex} = c_v^{eq} \left(\frac{Q_{vf}}{T^2}\right) \Delta T \quad (21)$$

4.3.1. Model for Self Diffusion

Diffusion occurs by the motion of defects like vacancies and interstitial atoms and by atomic exchange. But vacancy motion is the predominant diffusion mechanism due to the lower activation energy of vacancy formation (Fridel, 1964). The self diffusion coefficient can be written according to Reed-Hill and Abbaschian (1991) as,

$$D_l = a^2 \nu e^{\frac{\Delta S_{vm} + \Delta S_{vf}}{k}} e^{-\frac{Q_{vm} + Q_{vf}}{kT}} = D_{l0} e^{-\frac{Q_v}{kT}} \quad (22)$$

where, a is the lattice constant, ν is the lattice vibration frequency, ΔS_{vm} is the entropy increase due to the motion of a vacancy, Q_{vm} is the energy barrier to be overcome for vacancy motion and D_{l0} is the activity factor of lattice diffusion.

Vacancy migration leads to vacancy annihilation and it follows an Arrhenius type relation as below.

$$D_{vm} = a^2 \nu e^{\frac{\Delta S_{vm}}{k}} e^{-\frac{Q_{vm}}{kT}} \quad (23)$$

Introducing the equilibrium concentration of vacancy from equation (17), self diffusivity can be written as,

$$D_l = c_v^{eq} D_{vm} \quad (24)$$

Thus the self-diffusivity is the product of vacancy diffusivity and its equilibrium concentration. This can be rewritten generically for any concentration of vacancy as,

$$D_l^* = \frac{c_v}{c_v^{eq}} D_l \quad (25)$$

Lattice diffusivity of α and β phases differ in many order of magnitude which results in a jump at the β-transus temperature (Mishin and Herzig, 2000). This transition is modelled by scaling the diffusivity with the volume fraction of each phases.

$$D_l = D_\alpha \cdot (1-f)^w + D_\beta \cdot f^w \quad (26)$$

where $f = f(T)$ is the volume fraction of β phase.

Lattice diffusion is responsible for climb at high temperatures. However at intermediate temperatures, diffusion along dislocation lines, referred to as core or pipe diffusion has a larger effect on climb (Prinz et al., 1982). While studying the static grain growth of fine grained Ti-6Al-4V ($g < 2\mu$m), Johnson et al. (1998) has concluded that grain boundary and pipe diffusion are the controlling mechanisms at temperatures less than $0.5T_{melt}$. The effect of grain boundary diffusion can be neglected in the proposed model because of a much larger grain size of the material considered. Reed-Hill and Abbaschian (1991) proposed an Arrhenius type equation for grain boundary diffusion similar to equation (23). Since the basic mechanisms of grain boundary and dislocation core diffusion are the same (Shewmon, 1963), a similar formulation can be employed here.

$$D_p = D_{p0} e^{-\frac{Q_p}{kT}} \quad (27)$$

where, D_{p0} is the frequency factor and Q_p is the activation energy.

The total diffusive flux in the material is enhanced by the short circuit diffusion which is dependant on the relative cross sectional area of pipe and matrix. According to the model proposed by Porter and Easterling (1992); Militzer et al. (1994), the apparent diffusivity can be written as

$$D_{app} = D_l + N D_p \quad (28)$$

where, N is the cross sectional area of pipes per unit area of matrix.

$$N = \frac{n_a^p n_\rho}{N_a^l} \tag{29}$$

where, n_a^p is the number of atoms that can fill the cross-sectional area of a dislocation, n_ρ is the number of dislocations intersecting a unit area and N_a^l is the number of atoms per unit area of lattice.

4.4. Stress-Update

To compute the flow stress evolution for arbitrary paths, a radial return algorithm can be used (Simo and Taylor, 1986; Simo and Hughes, 1998). This requires hardening modulus and updated internal variables for each time increment. In the proposed model, $\sigma_y = \sigma_y(\bar{\varepsilon}^p, \rho_i, c_v)$ where ρ_i and c_v are described by a coupled set of differential equations. These internal variables can be written in vector form as $\mathbf{q}^T = [q_1, q_2] = [\rho_i, c_v]$. An implicit iterative procedure is used in every time increment to calculate its evolution as given below.

$$\mathbf{H}^T = [H_1, H_2] = 0 \tag{30}$$

$$H_1 = \Delta q_1 - \left[\frac{m}{b\Lambda}\Delta\bar{\varepsilon}^p - \Omega q_1 \Delta\bar{\varepsilon}^p - 2c_\gamma D_l q_2 \frac{Gb^3}{kT}\left(q_1^2 - \rho_{eq}^2\right)\rho_{i0}\Delta t\right] \tag{31}$$

$$H_2 = \Delta q_2 - \left[\chi\frac{\Omega_0 m\alpha G b}{Q_{vf}}\sqrt{q_1}\Delta\bar{\varepsilon}^p + \zeta\frac{c_j\Omega_0}{4b^3}\Delta\bar{\varepsilon}^p - \frac{D_{vm}}{\Lambda^2}\left(q_2 - c_v^{eq}\right)\Delta t + c_v^{eq}\left(\frac{Q_{vf}}{T^2}\right)\Delta T\right] \tag{32}$$

The iterative change in $\mathbf{q}$ can be written as,

$$d\mathbf{q} = -\left[\frac{\partial \mathbf{H}_{(i)}}{\partial \mathbf{q}}\right]^{-1}\mathbf{H}_{(i)} \tag{33}$$

where, i is the iteration counter. The value of the state variables can be updated as

$$\mathbf{q}_{(i+1)} = \mathbf{q}_{(i)} + d\mathbf{q} \tag{34}$$

The hardening modulus is defined as,

$$H' = \frac{d\sigma_y(\mathbf{q})}{d\bar{\varepsilon}^p} = \frac{\partial\sigma_y}{\partial\mathbf{q}}\frac{\partial\mathbf{q}}{\partial\bar{\varepsilon}^p} = \frac{\partial\sigma_G}{\partial\rho_i}\left[\frac{\partial\rho_i}{\partial\bar{\varepsilon}^p} + \frac{\partial\rho_i}{\partial c_v}\frac{\partial c_v}{\partial\bar{\varepsilon}^p}\right] + \frac{\partial\sigma^*}{\partial\bar{\varepsilon}^p} \tag{35}$$

5. Optimization of the model

The parameters for the model are obtained using an in-house Matlab® based toolbox. This toolbox uses Matlab®'s constrained minimization routine and can handle multiple experiments for optimization (Domkin and Lindgren, 2003). The shear modulus is computed

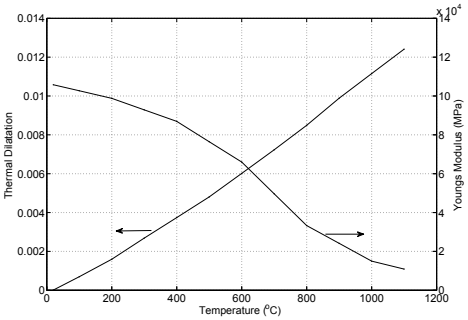

Figure 1: Thermal dilatation and Youngs modulus.

according to equation (4) using the temperature dependant Youngs modulus given in figure 1. These values are obtained from isothermal tension tests using 0.2% offset. The Poisson ratio is assumed to be 0.3 for all temperatures. Strain has contributions from mechanical and thermal loads. Figure 1 shows the thermal strain measured using a differential expansion dilatometer.

According to Hernan et al. (2005), the entropy of vacancy migration for HCP metals lies in the range $(0.9 - 1.6)k$. Here ΔS_{vm} is assumed to be equal to k. The activation energy of vacancy formation (Q_{vf}), measured by Novikov et al. (1980) for elemental Ti is used in this work. Conrad (1981) measured the dislocation density of undeformed Ti alloy with (0.1 - 1.0) at% O_{eq} to be of the order of $10^{13}\mathrm{m}^{-2}$. This should apply for Ti-6Al-4V also. Figure 2 shows the apparent diffusivity of Ti-6Al-4V for different values of dislocation density which correspond to annealed and deformed material. Enhanced diffusivity due to pipe diffusion has a significant effect at low temperature ($< 0.5T_{melt}$). At high temperature, it is the lattice diffusivity which has significance. The measurement of Mishin and Herzig (2000) show the self diffusion of Ti in α and β phases whereas the measurement of Semiatin et al. (2003) show diffusion of Al in β phase of Ti-6Al-4V. The activity factor of pipe diffusion (D_{p0}) is assumed to be of the same order as that of lattice diffusion. The different parameters of the model obtained after fitting to experiments are

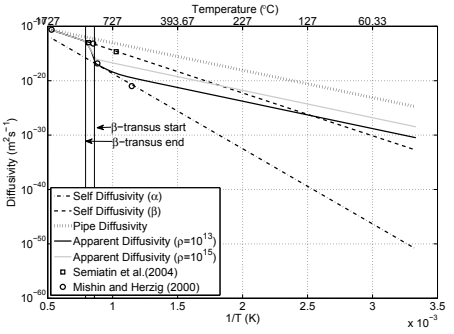

Figure 2: Self diffusion.

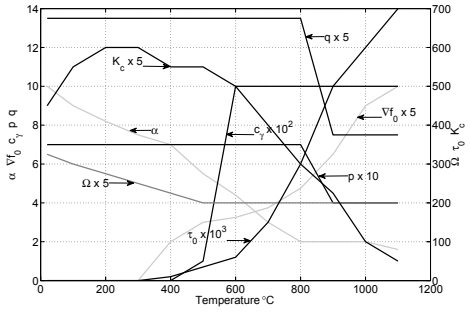

Figure 3: Temperature dependant parameters for the model.

Parameter	Dimension	Value	Reference
T_{melt}	°C	1600	
$T_{\beta-transus}$	°C	890	
k	JK^{-1}	$1.38 \cdot 10^{-23}$	
b	m	$2.95 \cdot 10^{-10}$	a
ΔS_{vm}	JK^{-1}	$1.38 \cdot 10^{-23}$	f
$D_{\alpha 0}$	m^2s^{-1}	$5.0 \cdot 10^{-6}$	d
$D_{\beta 0}$	m^2s^{-1}	$3.0 \cdot 10^{-7}$	d
D_{p0}	m^2s^{-1}	10^{-8}	f
Q_{vf}	J	$1.9 \cdot 10^{-19}$	b
Q_{vm}	J	$2.49 \cdot 10^{-19}$	a
Q_{β}	J	$2.5 \cdot 10^{-19}$	d
Q_{p}	J	$1.61 \cdot 10^{-19}$	a
n_a^p	-	2	e
n_ρ	-	ρ_i	e
N_a^l	-	10^{19}	f
Ω_0	m^3	$1.76 \cdot 10^{-29}$	a
g	m	$20.0 \cdot 10^{-6}$	e
s_∞	m	$6.0 \cdot 10^{-7}$	g
$\dot{\varepsilon}_{ref}$	s^{-1}	10^6	a
ρ_{i0}	m^{-2}	10^{13}	c
ρ_{eq}	m^{-2}	10^{10}	g

[a] Frost and Ashby (1982)
[b] Novikov et al. (1980)
[c] Conrad (1981)
[d] Mishin and Herzig (2000)
[e] Calculated or Measured Value
[f] Assumed Value
[g] Optimization Parameter

Table 3: Constant parameters for the model.

shown in the figure 3. The parameters p and q jumps in magnitude between (800 and 900)°C. This can be attributed to the onset of β-transition.

6. Model and experiments

Comparison of experiments and predictions of the model are plotted in the figures 4, 5, 6 and 7. The dots denote experiments and lines denote predictions. Compression tests performed at the nominal temperatures (20, 100, 200, 300, 400, 500, 600, 700, 800, 900, 1000 and 1100)°C have been used to calibrate the model. The actual temperature recorded from the thermocouple deviated slightly from the nominal values and was accounted for in the computation. The compression tests performed at 20°C to 500°C resulted in hardening followed by fracture and at temperatures between 600°C to 900°C resulted in flow softening after the initial hardening. The deformation mechanisms leading to flow softening is not well understood. Park et al. (2008) has reported that grain boundary sliding (GBS) controlled by grain boundary diffusion is the dominant mechanism responsible for this behavior. Ti-6Al-4V undergoes dynamic recrystallization (DRx) at elevated temperatures (Abe et al., 2003). DRx can lead to flow softening because the new grains have lower dislocation density than the existing ones. The tests from 1000°C to 1100°C showed elastic-perfectly-plastic behavior. Between 20°C to 500°C, the flow stress is less sensitive to strain rate. Comparison of stress relaxation measurements done by Donachie (1988) and the model predictions are given in figure 7. Though, the exact boundary conditions of the experiments and the composition of the alloy are not known, this comparison demonstrates the capacity of the model to compute the decay of stress with time. The model underestimates initial relaxation of stress. This maybe ascribed to mechanisms of GBS

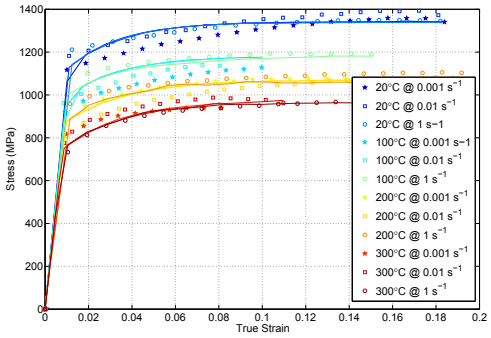

Figure 4: Measured and computed stress-strain curve for 20°C to 300°C.

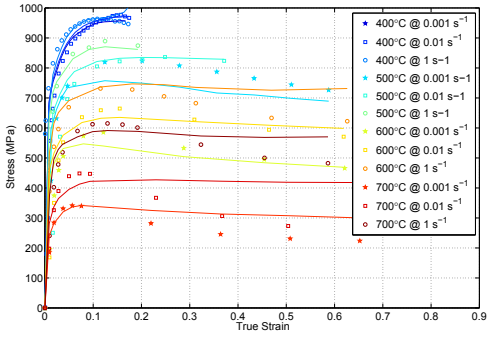

Figure 5: Measured and computed stress-strain curve for 400°C to 700°C.

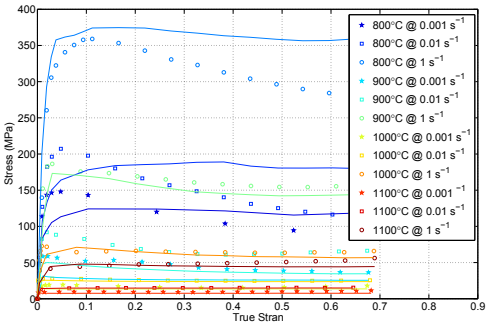

Figure 6: Measured and computed stress-strain curve for 800°C to 1100°C.

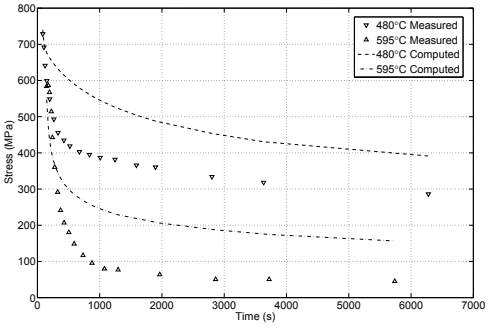

Figure 7: Measured and computed stress relaxation at 480°C and 595°C.

or DRx responsible for flow softening which is not included in this work.

7. Conclusions

A constitutive model based on the physics of the material behavior is developed. The model can give predictions with sufficient accuracy for simulations of various manufacturing processes like forming, welding, metal deposition and heat treatment. Some of the parameters used in the model are available from measurements outside the domain of classical mechanical testing. Since some of these parameters are not available for this specific alloy, the data for elemental Ti has been used here. The logic for stress update described here is directly applicable for large scale simulations.

Some additional measurements are necessary to validate the various submodels employed here. This task is already in progress. Since this flow stress model follow a clear physical framework, new submodels can be added with relative ease.

Acknowledgments

This work was performed with the financial support from VERDI; a project under the sixth framework programme of the EU. The experiments using the Gleeble® machine were done at the Materials Engineering Laboratory, University of Oulu. Dr. Mahesh C. Somani and other staff were of great help in conducting this timely and accurately.

A. Appendix

The iterative solution procedure for the internal state variables in equation (33) involve the computation of

the following derivatives.

$$\frac{\partial H_1}{\partial q_1} = 1 + \Omega q_1 \Delta\bar{\varepsilon}^p + 4c_\gamma D_l \frac{q_2}{c_v^{eq}} \frac{Gb^3}{kT} q_1 \Delta t \quad (36)$$

$$\frac{\partial H_1}{\partial q_2} = -2c_\gamma D_l \frac{1}{c_v^{eq}} \frac{Gb^3}{kT} \left(q_1^2 - \rho_{eq}^2\right) \Delta t \quad (37)$$

$$\frac{\partial H_2}{\partial q_1} = -0.5\chi \frac{\Omega_0 m\alpha Gb}{Q_{vf}\sqrt{q_1}} \Delta\bar{\varepsilon}^p \quad (38)$$

$$\frac{\partial H_2}{\partial q_2} = 1 + \frac{D_{vm}}{\Lambda^2} \Delta t \quad (39)$$

The expression for hardening modulus in equation (35) requires evaluation of the following derivatives.

$$\frac{\partial \sigma_G}{\partial \rho_i} = \frac{m\alpha Gb}{2\sqrt{q_1}} \quad (40)$$

$$\frac{\partial \rho_i}{\partial \bar{\varepsilon}^p} = \frac{m}{b\Lambda} - \Omega q_1 \quad (41)$$

$$\frac{\partial \rho_i}{\partial c_v} = -2c_\gamma D_l \frac{1}{c_v^{eq}} \frac{Gb^3}{kT} \left(q_1^2 - \rho_{eq}^2\right) \Delta t \quad (42)$$

$$\frac{\partial c_v}{\partial \bar{\varepsilon}^p} = \chi \frac{\Omega_0 m\alpha Gb}{Q_{vf}} \sqrt{q_1} + \zeta \frac{c_j \Omega_0}{4b^3} \quad (43)$$

$$\frac{\partial \sigma^*}{\partial \bar{\varepsilon}^p} = \frac{\sigma_{th} \left(\frac{kT log\left(\frac{\dot{\varepsilon}^{ref}}{\dot{\bar{\varepsilon}}^p}\right)}{\Delta f_0 Gb^3} \right)^{\frac{1}{q}}}{pq\bar{\varepsilon}^p log\left(\frac{\dot{\varepsilon}^{ref}}{\dot{\bar{\varepsilon}}^p}\right) \Delta t} \times \left(1 - \left(\frac{kT log\left(\frac{\dot{\varepsilon}^{ref}}{\dot{\bar{\varepsilon}}^p}\right)}{\Delta f_0 Gb^3} \right)^{\frac{1}{q}} \right)^{\frac{1}{p}-1} \quad (44)$$

References

Abe, H., Furuhara, T., Maki, T., 2003. Dynamic recrystallization of Ti-6Al-4V alloy. Current Advances in Materials and Processes 16 (6), 1479.

Bergström, Y., 1969. Dislocation model for the stress-strain behaviour of polycrystalline alpha-iron with special emphasis on the variation of the densities of mobile and immobile dislocations. Materials Science & Engineering 5, 193–200.

Bergström, Y., 1983. The plastic deformation of metals – a dislocation model and its applicability. Reviews on Powder Metallurgy and Physical Ceramics (2/3), 79–265.

Conrad, H., 1981. Effect of interstitial solutes on the strength and ductility of titanium 26 (2-4), 123.

de Meester, B., Döner, M., Conrad, H., 1975. Deformation kinetics of the Ti-6Al-4V alloy at low temperatures. Metallurgical and Materials Transactions A 6 (1), 65–75.

Domkin, K., Lindgren, L.-E., Apr. 2003. Dislocation density based models of plastic hardening and parameter identification. In: The 7th International Conference on Computer Plasticity. COMPLAS.

Donachie, J. M. J., 1988. Titanium - A Technical Guide. ASM International.

Fridel, J., 1964. Dislocations. Vol. 3 of International Series of Monographs on Solid State Physics. Pergamon Press.

Frost, H. J., Ashby, M. F., 1982. Deformation-Mechanism Maps: The Plasticity and Creep of Metals and Ceramics. Paperback.

Hernan, R. D., Maria, G. L., Maria, M. A., 12 2005. Self-diffusion in the hexagonal structure of zirconium and hafnium: computer simulation studies. Materials Research 8, 431–434.

Holt, D. L., 1970. Dislocation cell formation in metals. Journal of applied physics 41 (8), 3197, 0021-8979.

James, C. W., Lutjering, G., 2003. Titanium. Springer - Verlag.

Johnson, C. H., Richter, S. K., Hamilton, C. H., Hoyt, J. J., 1998. Static grain growth in a microduplex Ti-6Al-4V alloy. Acta Materialia 47 (1), 23–29.

Kailas, S. V., Prasad, Y. V. R. K., Biswas, S. K., 1994. Flow instabilities and fracture in Ti-6Al-4V deformed in compression at 298-673k. Metallurgical and Materials Transactions A 25A (10), 2173–2179, pdf of this document is not availabe.

Kocks, U., 1976. Laws for work-hardening and low-temperature creep. Journal of Engineering Materials and Technology, Transactions of the ASME 98 Ser H (1), 76–85.

Kocks, U. F., Argon, A. S., Ashby, M. F., 1975. Thermodynamics and Kinetics of Slip. Vol. 19 of Progress in Material Science. Pergamon Press.

Lindgren, L.-E., Domkin, K., Sofia, H., June 2008. Dislocations, vacancies and solute diffusion in physical based plasticity model for aisi 316l. Mechanics of Materials 40 (11), 907–919.

Liu, Z., Welsch, G., 1988. Literature survey on diffusivities of oxygen, aluminum, and vanadium in alpha titanium, beta titanium, and in rutile. Metallurgical and Materials Transactions A 19 (4), 1121–1125.

Majorell, A., Srivatsa, S., Picu, R. C., 2002. Mechanical behavior of Ti-6Al-4V at high and moderate temperatures–part i: Experimental results. Materials Science and Engineering A 326 (2), 297–305.

Mecking, H., Estrin, Y., 1980. The effect of vacancy generation on plastic deformation. Scripta Metallurgica 14 (7), 815.

Mecking, H., Kocks, U., 1981. Kinetics of flow and strain-hardening. Acta Metallurgica 29 (11), 1865–1875.

Militzer, M., Sun, W. P., Jonas, J. J., 1994. Modelling the effect of deformation-induced vacancies on segregation and precipitation. Acta Metallurgica et Materialia 42 (1), 133.

Mishin, Y., Herzig, C., Feb. 2000. Diffusion in the ti-al system. Acta Materialia 48 (3), 589–623.

Nemat-Nasser, S., Guo, W.-G., Cheng, J. Y., 1999. Mechanical properties and deformation mechanisms of a commercially pure titanium. Acta Materialia 47 (13), 3705.

Novikov, I. I., Roshchupkin, V. V., Semashko, N. A., Fordeeva, L. K., 1980. Experimental investigation of vacancy effects in pure metals. Journal of Engineering Physics and Thermophysics V39 (6), 1316.

Orowan, E., 1948. In: Symposium on Internal Stresses in Metals and Alloys. Institute of Metals, p. 451.

Park, C. H., Ko, Y. G., Park, J.-W., Ko, Y. G., May 2008. Enhanced superplasticity utilizing dynamic globularization of Ti-6Al-4V alloy. Materials Science and Engineering: A.

Picu, R. C., Majorell, A., 2002. Mechanical behavior of Ti-6Al-4V at high and moderate temperatures–part ii: constitutive modeling. Materials Science and Engineering A 326 (2), 306–316.

Porter, D. A., Easterling, K. E., 1992. Phase Transformations in Met-

als and Alloys, 2nd Edition. CRC Press.
Prinz, F., Argon, A. S., Moffatt, W. C., 1982. Recovery of dislocation structures in plastically deformed copper and nickel single crystals. Acta Metallurgica 30 (4), 821–830.
Reed-Hill, R. E., Abbaschian, R., 1991. Physical Metallurgy Principles, 3rd Edition. PWS Publishing Company.
Sandstrom, R., Lagneborg, R., 1975. A model for hot working occurring by recrystallization. Acta Metallurgica 23 (3), 387.
Seeger, A., 1956. The mechanism of glide and work hardening in fcc and hcp metals. In: Fisher, J., Johnston, W. G., Thomson, R., Vreeland, T. J. (Eds.), Dislocations and Mechanical Properties of Crystals. pp. 243–329.
Semiatin, S., Knisley, S., Fagin, P., Barker, D., Zhang, F., 2003. Microstructure evolution during alpha-beta heat treatment of Ti-6Al-4V. Metallurgical and Materials Transactions A 34 (10), 2377–2386.
Seshacharyulu, T., Medeiros, S. C., Frazier, W. G., Prasad, Y. V. R. K., 2002. Microstructural mechanisms during hot working of commercial grade Ti-6Al-4V with lamellar starting structure 325 (1-2), 112.
Shewmon, P. G., 1963. Diffusion in solids. McGraw-Hill series in materials science and engineering. McGraw-Hill.
Simo, J., Hughes, T. J. R., 1998. Computational Inelasticity, 1st Edition. Vol. 7 of Interdisciplinary Applied Mathematics. Springer.
Simo, J. C., Taylor, R. L., 1986. A return mapping algorithm for plane stress elastoplasticity. International Journal for Numerical Methods in Engineering 22 (3), 649–670.
Tiley, J. S., 2002. Modeling of microstructure property relationships in Ti-6Al-4V. Ph.D. thesis, Ohio State University.